A REPORT FROM

OWENS-ILLINOIS TECHNICAL CENTER

FORM NO. 605-K

CONSUMER & TECHNICAL PRODUCTS DIVISION
RESEARCH, DEVELOPMENT & ENGINEERING

OWENS ILLINOIS
GENERAL OFFICES (O) TOLEDO 1, OHIO

DISCLAIMER NOTICE

THIS DOCUMENT IS THE BEST QUALITY AVAILABLE.

COPY FURNISHED CONTAINED A SIGNIFICANT NUMBER OF PAGES WHICH DO NOT REPRODUCE LEGIBLY.

SPONSORED BY:

ADVANCED RESEARCH PROJECTS AGENCY

ARPA ORDER NO. 1441

PROGRAM CODE 9D10

SEMI-ANNUAL TECHNICAL REPORT

By: N. L. Boling, L. Sparoudis, and F.R. Wengert

DAMAGE THRESHOLD STUDIES OF GLASS LASER MATERIALS

31 JULY 1971

CONTRACT NO. DAHC15-69-C-0303

CONTRACT DATE	30 JUNE 1969
CONTRACT EXPIRATION	30 JUNE 1972
CONTRACT AMOUNT	$601,967

CONSUMER & TECHNICAL PRODUCTS DIVISION

OWENS-ILLINOIS, INC.

TOLEDO, OHIO

PHONE: (419) 242-6543, EXTENSION 33003

FOREWORD

The work outlined in this semi-annual report was performed under Contract DAHC15-69-C-0303, ARPA Order 1441, and Program Code P9D10. The work was performed within the Consumer and Technical Products Division of Owens-Illinois, Inc., Toledo, Ohio and covers the time period from 1 January 1971 through 30 June 1971.

The principal investigator for the program is N. L. Boling and the program manager is H. A. Lee. The thermodynamics of the melting of laser glass in platinum is being conducted by L. Spanoudis under the direction of P. R. Wengert. This contract is administered by the Chief, Defense Contract Administration Services Office, Toledo, Ohio. Dr. Maurice J. Sinnott, Director for Materials Sciences, ARPA, is the Contracting Officer's Technical Representative.

TABLE OF CONTENTS

ABSTRACT

This report discusses surface and particulate damage to laser glass by high power laser pulses. Surface damage is studied through high speed holography. Holograms of damaged samples are taken within a few hundred nanoseconds after damage. The plasmas and acoustic disturbances associated with damage and visible in these holograms are analyzed in detail. The possibility of eliminating damaging particles from laser glass is examined in a theoretical and experimental investigation. Melting of glass under reduced partial pressure of oxygen in platinum is presented as a method for accomplishing this elimination. Also discussed in this report is the design of a high power, high energy, TEM_{oo} mode laser to be used in damage studies.

1. SUMMARY

The work described in this report is a continuation of the work reported in the semi-annual report of 31 December, 1970. The reader is referred to that report for orientation to the work being performed under this contract. Only results and modifications of the last six months will be discussed herein.

On the investigation of surface damage, a high speed holographic study of the damage process has been made. Holograms taken with a Q-switched ruby laser show damaged samples at various times, nominally a few hundred nanoseconds, after the damaging pulse has passed through them. The surface plasmas are clearly visible in the holograms. Acoustic disturbances from the damage sites can also be easily seen.

Using the holograms the ion and electron temperatures, electron densities, and plasma expansion velocities can be obtained. Ion temperatures of 30,000°K are measured approximately 200ns after the damaging pulse. Electron densities in the plasma at the time of the damage are estimated to be typically greater than 10^{21} electrons/cm^3. Plasma expansion velocities greater than 10^5cm/sec are found 200ns after the damage occurs.

A possible surface damage mechanism involves the radiation of the surface by ultraviolet photons from the surface plasma initially formed by desorption of impurities at the surface. This radiation renders the surface highly absorbent to the incident laser pulse.

A great deal of progress has been realized in the design and construction of a high power, high energy laser operating in the TEM_{oo} mode. This laser is meant to be used in future damage studies. The oscillator is essentially complete and is reported on here. Energies of 200-300 millijoules in 20-40ns pulses are expected to be obtained from the oscillator.

In order to study damage at shorter pulse lengths, an optical shutter will be installed in the TEM_{oo} mode laser. This shutter, will allow attainment of pulses variable in temporal width from approximately 2-40ns.

Work has continued on the thermodynamics study of melting laser glass in platinum crucibles. Some of the results obtained in the past six months are as follows:

1. Both theoretical consideration and a change in the P_{O_2} during the melting history of the samples used in the Battelle study indicate that the partial pressure of oxygen is an important parameter to control.

2. An extensive literature search has been compiled on the activities of metals in platinum and on the activities of oxides in glass.

3. Using various theoretical models, the thermodynamic activities of metals in platinum and of oxides in laser glass cannot be estimated within two orders of magnitude.

4. A technique was developed which enables the simultaneous determination of the activities of several oxides in a glass composition and the activities of corresponding metals in dilute solutions of one of the more precious metals, such as Pt, Pd, Rh, and Ir.

5. The thermodynamic activities of Li_2O, CaO, Al_2O_3, and SiO_2, have been determined in an Li_2O-CaO-SiO_2-Nd_2O_3 laser glass at 3 P_{O_2}'s. The activities of the corresponding metals in platinum have also been determined.

6. It has experimentally been determined that the Li_2O-CaO-SiO_2-Nd_2O_3 laser glass can be melted in platinum at an oxygen partial pressure of 10^{-10} atms. without crucible attack. Using the derived thermodynamic data, it appears that oxygen partial pressures in the 10^{-12} atm. range would cause platinum crucible failure at 1700°K (2000°F).

2. HOLOGRAPHIC STUDY OF SURFACE DAMAGE

2.1. Damage Mechanisms

Several investigators have hypothesized various mechanisms to be responsible for surface damage of glass subjected to a high power laser pulse. Some of these are as follows:

1.) The electrostrictive interaction between the laser beam and the glass causes a radial constriction of the glass. The Poisson effect resulting from the squeeze causes a compression wave to be propagated along the laser beam. When this compression reaches the surface the unloading effect causes rupture of the surface.

2.) Stimulated Brillouin scattering initiates and amplifies an acoustic wave which propagates along the forward direction of the beam. This wave ruptures the surface upon incidence.

3.) The surface plasma, which invariably accompanies surface damage and which forms in the first few nanoseconds of the laser pulse, rapidly expands upon partial absorption of the tail end of the pulse. This expansion creates a shock wave which damages the surface. The plasma originally stems from desorption of impurities from the surface.

4.) The surface plasma of (3) bombards the surface with thermally energetic ions. This results in thermal erosion of the surface.

Self trapping could play a role in any of these by increasing the energy density of the laser beam. In fact, observations indicate that self trapping is very often, if not always, associated with surface damage. Thus any of the various mechanisms hypothesized to cause self trapping could also be considered, at least indirectly, a cause of surface damage.

2.2 Experimental Arrangement

As a means of studying the damage process near the time the damage occurs, we have been using high speed holography. Figure 1 is a diagram of the essentials of the experimental arrangement. A glass oscillator-amplifier system emits a 40 ns pulse of up to eight joules. This is passed through a lens of 150, 25 or 10 cm focal length and then is incident upon the glass sample to be studied. The sample is a one inch cube of ED-2 in most cases. When the 150 cm lens is used, the sample is placed about 130 cm from the lens. When the 25 cm lens is used the sample is about 20 cm from the lens. When the 10 cm lens is used the exit face of the sample is generally placed just before the focal point of the lens. With these arrangements the energy density varies from just above the damage threshold with the 150 cm lens to well above 150 j/cm^2 with the 10 cm lens.

At a selected time after the damage pulse from the glass laser a hologram is made of the sample with a ruby laser which emits a TEM_{00} pulse of 20 ns duration. The time interval between the damage pulse and the hologram pulse can be varied from 0 to several microseconds. Up to 500 ns the interval can be controlled to within 10 ns. After the photographic plate on which the hologram is made is developed, the virtual or real image of the sample can be studied or photographed at leisure.

Two types of holograms are made with this apparatus, single exposure and double exposure. The single exposure, in which the ruby laser is fired only once, results in a shadowgram superimposed on the hologram of the sample.

The shadowgram shows regions in which the optical density changes rapidly in space. The double exposure technique requires that a hologram first be made of the sample without the damaging pulse. Next, the sample is subjected to the damaging pulse and another hologram is made, using the same photographic plate, after the selected time interval. The result is a hologram of the sample with fringes due to its change in state during the time between the two holograms. A shadowgram is also present in the resulting hologram.

2.3 Experimental Results

Introduction

Before describing any of the results obtained it should be noted that this was not a study of the damage threshold per se. The intent thus far has been to gain experience in the holographic technique as it applies to this particular problem and to study damage mechanisms. In the latter case it seems worth mentioning, since the point seems so often missed, that much can be learned about a physical process which is of interest within certain limits by studying that process well outside those limits. Thus studies of gross damage could well lead to an understanding of the less severe damage encountered in practice.

Holograms

In this subsection, we present some photographs of holograms representative of those made in this study. Interpretations of these will be made as appropriate.

Figure 2 is a photo taken of the virtual image of a double exposure hologram. The time delay between the damaging shot and the pulse which made the ogram was 190 ns. The lens used to focus the damaging beam was the focal length lens.

Both exit and entrance plasmas can be clearly seen in the photo. (The exit is to the right in this photo as in all others presented herein). Note the clarity of the fringe pattern in the entrance plasma while the exit

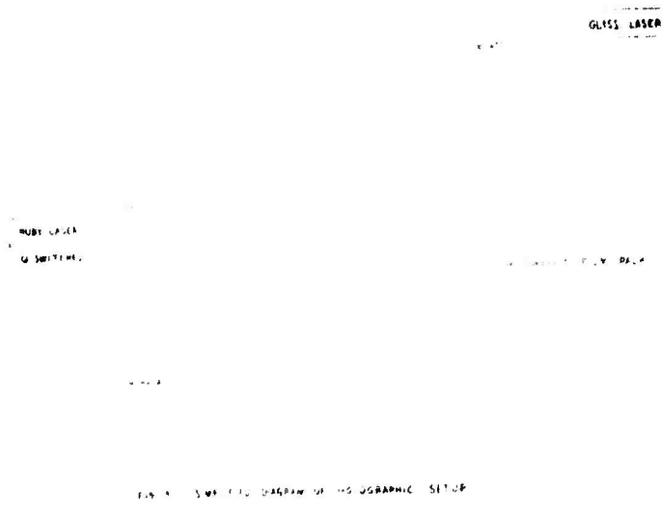

FIGURE 1

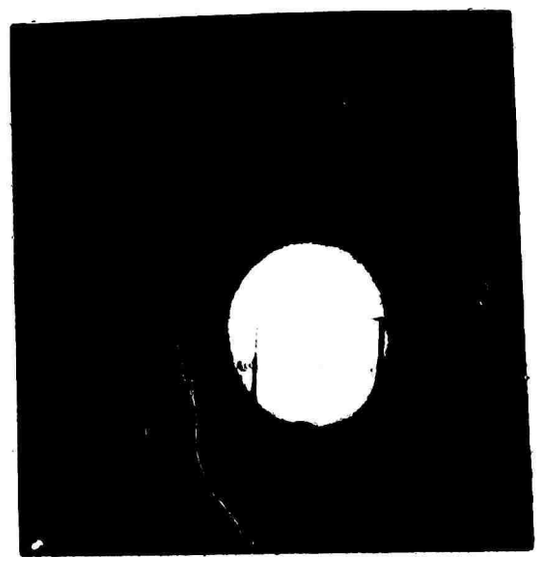

FIGURE 2

plasma has a different character. Close examination of the photo reveals two acoustic waves propagating into the sample from the damage site on the exit. No such disturbance is seen at the entrance face.

Also visible in the photo is an internal damage track which terminates at the exit face. This track was actually formed during a previous damaging shot at a different position in the cube and only appears in the photo to be associated with the shot of which this hologram was made.

Figures 3 and 4 are microphotographs of the entrance and exit surface damage respectively. There is a definite cracking of the entrance surface, but still no acoustic wave is associated with this surface in this case, at least not one of great enough intensity to be detected on the hologram.

Figure 5 shows a photograph of a hologram taken with a time delay of 1600 ns after the damaging shot. No exit plasma is visible but there is a definite plasma at the entrance face. This is more obvious in Figure 6 which is a photo taken with a camera mounted above the sample. The shutter of the camera is kept open during the damaging shot, so the result is an integrated photo of the damage process. No damage could be seen on either the entrance or exit of this sample.

It has been suggested that the appearance of a plasma at the surface should be used as a definition of damage. Here we have a plasma but no damage, at least no detectable damage. Even if one accepts the appearance of a plasma as a definition of damage, then the exit damage threshold is not always lower than the entrance damage threshold as is commonly accepted to be the case.

FIGURE 3

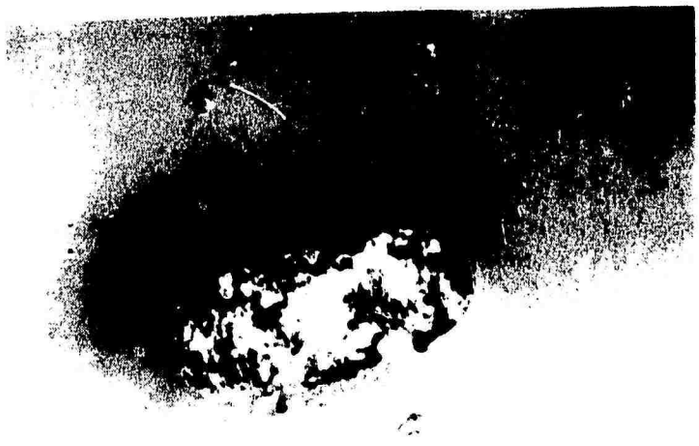

FIGURE 4

FIGURE

FIGURE

Figures 7, 8, 9, show photos of single exposure holograms with time delays of 190 ns, 900 ns, and 1425 ns respectively. These were all made with the damaging beam passing through the 10 cm lens, as was the hologram of Figure 10 which is a double exposure hologram (note the familiar fringe patterns of such holograms in the plasma).

In Figure 7 both exit and entrance plasmas as well as an interior damage track can be seen. An acoustic disturbance propagating away from the damage track is also present. Figures 8, 9, and 10 exhibit very clearly the exit plasma.

Three points should be noted concerning these last four photographs. First, two acoustic waves moving away from the damage sites in the exit faces and into the interiors of the samples are quite clear. In Figure 10 the second wave exhibits a "kink" where it meets the surface of the sample. A third and fourth wave can also be seen in Figure 10. No disturbances are seen moving from the interiors of the samples toward the surfaces. Second, parts of the plasmas are opaque to the ruby laser beam which was used to make the holograms. This is evinced by the black portions of the plasmas. Third, the plasmas exhibit a peculiar apiomorphic symmetry. This is most easily seen in Figures 9 and 10.

Concerning the first point, a disturbance in a small region of a solid will in general produce both longitudinal and transverse waves.

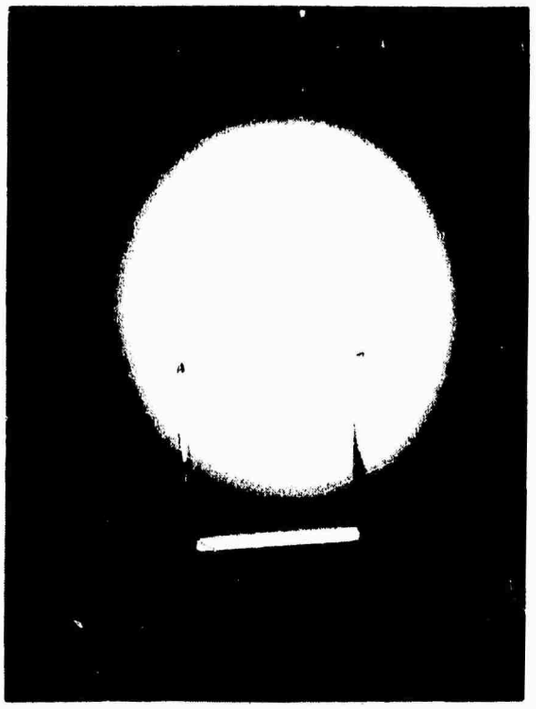

FIGURE 7

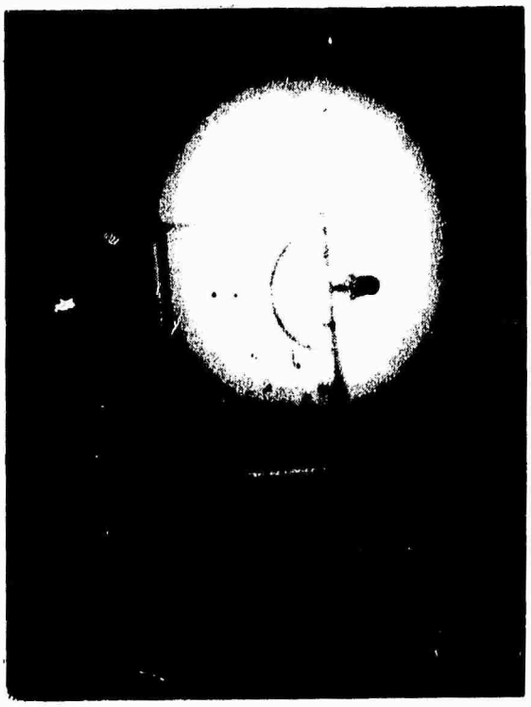

FIGURE 8

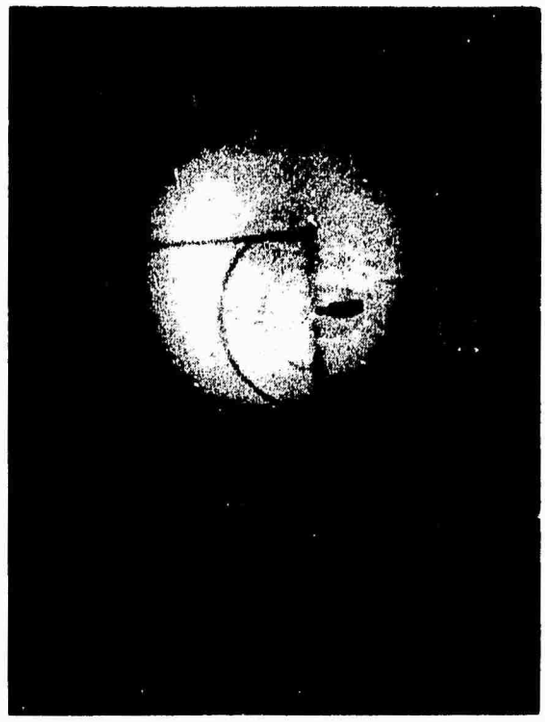

FIGURE 9

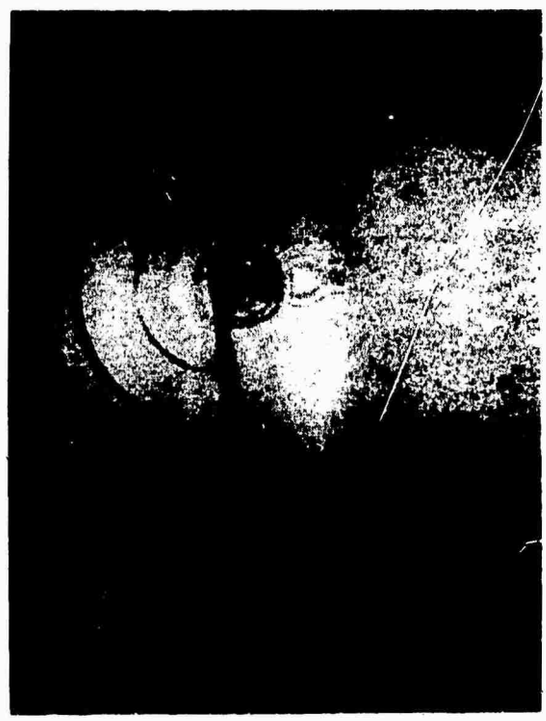

FIGURE 10

The speeds of these waves are given by

$$V_T = \left(\frac{\mu}{\rho}\right)^{1/2} \qquad (1)$$

$$V_L = \left[\frac{\left(K + \frac{4\mu}{3}\right)}{\rho}\right]^{1/2} \qquad (2)$$

where μ, ρ, and K are respectively the shear modulus, density, and bulk modulus of the material.

Using the measured values of these constants for ED-2, the glass used in these studies, we obtain from (1) and (2),

$$V_L = 6.46 \times 10^3 \text{ m/sec}$$

$$V_T = 3.77 \times 10^3 \text{ m/sec}$$

The ratio of these is 1.7.

If in Figures 8, 9, and 10, we measure the ratio of the distances which the two waves have traveled from the damage site, we obtain in all three cases 1.8. The leading wave, then, is a longitudinal wave and the trailing wave is transverse in character.

It is interesting to note that only one wave is apparent in the disturbance associated with the internal damage track. The wave is longitudinal as can be ascertained from the fact that it is of the same radius as the longitudinal, wave from the surface damage site. This has been noted in other holograms which show a wave from the internal damage track.

An explanation of the kink so apparent in the transverse wave of Figure 10 can be gleaned by calculating the speed of a Rayleigh (surface) wave in ED-2. This turns out to be 0.9 times the speed of a transverse wave. The relative distances of the kink and the transverse wave from the damage site are about right to support the contention that the kink is caused by a Rayleigh wave moving out from the damage site.

Turning now to the opaqueness of the exit plasma, we calculate the electron density which would be required in the plasma in order to render it opaque to the ruby laser wavelength. This given by

$$n_c = \frac{\varepsilon_o m \omega^2}{e^2} \qquad (3)$$

where m, ω, and e are respectively the mass of the electron, the angular frequency of the light, and the electroniccharge. Substituting values for these yields

$$n_c = 2.3 \times 10^{21} \text{ electrons/cm}^3$$

Thus if the electron density is higher than approximately $2 \times 10^{21}/\text{cm}^3$ in any region of the plasma, one would expect the plasma to be opaque to the ruby laser. In one respect it is reasonable to assume that this might be the case. Several investigators have noted that the latter part of the damaging laser pulse is apparently absorbed by the plasma. This implies that the electron density is greater than n_c, at least in the incipient stages of the plasma development. However, we note that the hologram of Figure 10, for example, was taken 1500 ns after the damaging pulse. That the electron density at this late time is still greater than n_c is doubtful.

Also, calculations (to be given further on in this report) show that each fringe in the plasma of Figure 10 should correspond to a change of about 3×10^{18} electrons/cm^3. This indicates, since there are three fringes across the plasma, that the density in the opaque region is about 10^{19}/cm^3, well below n_c.

Another, and perhaps more plausible, explanation of the opacity is that it is due to material expelled from the damage pit on the surface. This view is supported by the observation that entrance surface damage almost never takes the form of a pit, i.e., very little, if any, material is removed, and the entrance plasma is never observed to be opaque. Also supporting this explanation is Figure 11 which is a photo of a sample which has suffered gross damage. The delay time was 560 ns. The photo of Figure 12, taken with an open shuttered camera, indicates the great extent of the damage. The surface pit is about 3mm in diameter and 0.5 mm deep, so a large amount of material was expelled. Note the large region of opaqueness in the plasma. The evidence seems to indicate that material from the surface is being seen in these holograms.

We turn now to the third point raised above, the pear like shape of the plasmas of Figures 8, 9, and 10. The reason for this becomes immediately evident upon examination of Figure 13. This is a hologram of the spark created at the focus of the 10 cm lens while attempting to focus on the entrance surface. Obviously, the double pear shape is due to the focusing of the laser beam and is not a property of the interaction between the pulse and the surface. This, by the way, points up one of the dangers of measuring the damage threshold by using a focused beam. If the plasma is responsible for the damage, then it is easy

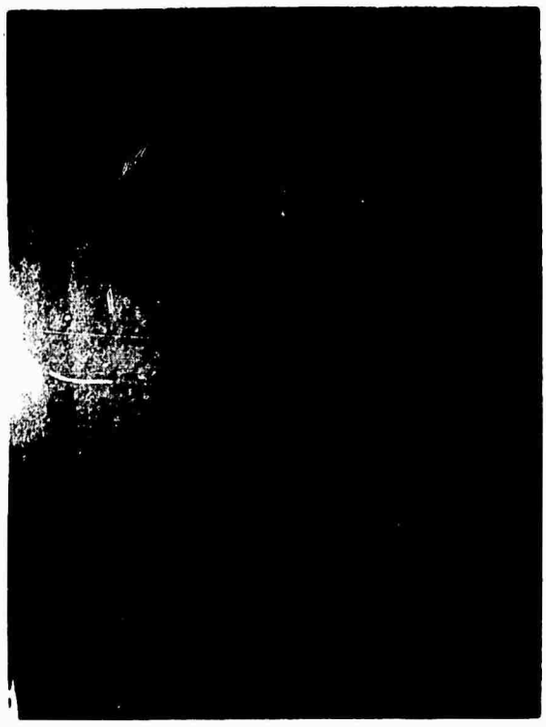

FIGURE 11

NOT REPRODUCIBLE

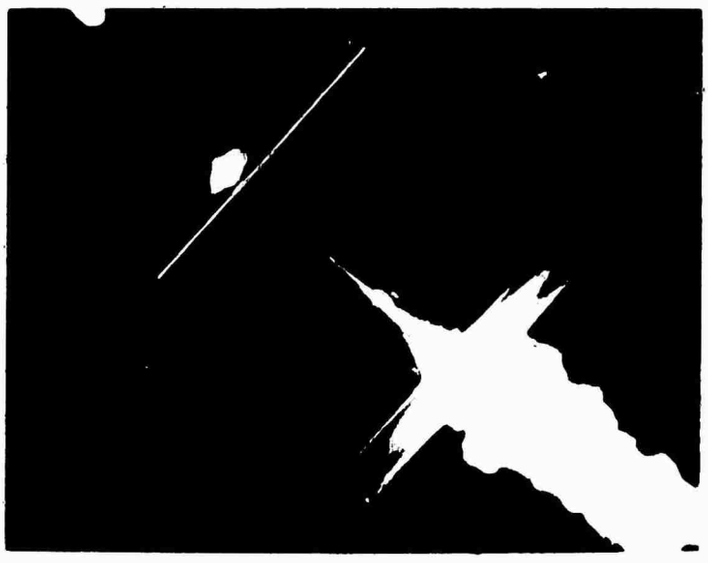

FIGURE 12

to imagine that the results would be affected by such a procedure. One has not only the interaction between the surface and the plasma created by adsorption from the surface to consider, but must also consider the interaction between the surface and the plasma created by focusing the beam near the surface.

Plasma Expansion Velocity and Ion Temperature

Figures 14 through 18 are all photos of double exposure holograms. The damaging beam was passed through the 25 cm lens and the energy density is about the same for every photo - approximately 100 j/cm^2 at the exit face. Delay times between the damaging pulse and the hologram pulse are, corresponding to the numerical order of the Figures, 270 ns, 580 ns, 880 ns, 1600 ns, and 1900ns. In short, the conditions for all five shots varied only in the delay time.

From this series of photos the rate of transverse (to the damaging laser beam) expansion of the plasma can be obtained by simply measuring the extent of the plasma at the various stages of its development. This expansion rate, which is the speed of sound in the plasma, depends upon the ion temperature of the plasma and is given by [6]

$$V_T = [\gamma(\gamma-1)\epsilon]^{1/2}, \qquad (3)$$

where ϵ is the internal energy per gram of the plasma and γ is the effective adiabatic exponent.

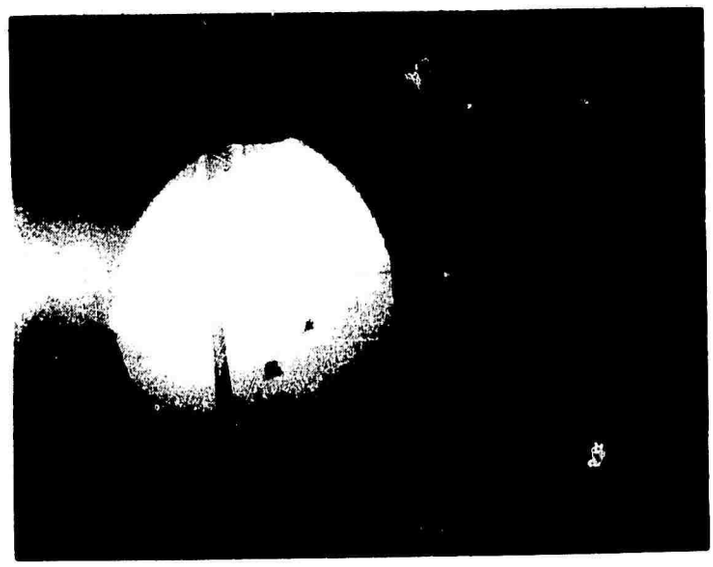

FIGURE 13

FIGURE 14

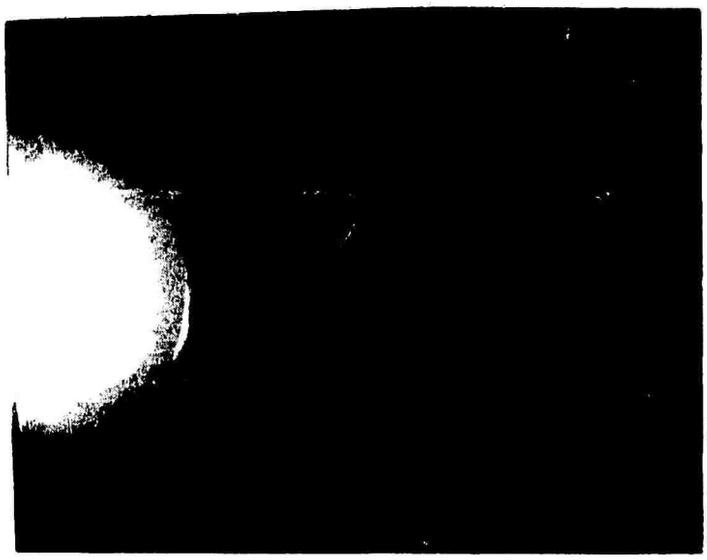

FIGURE 15

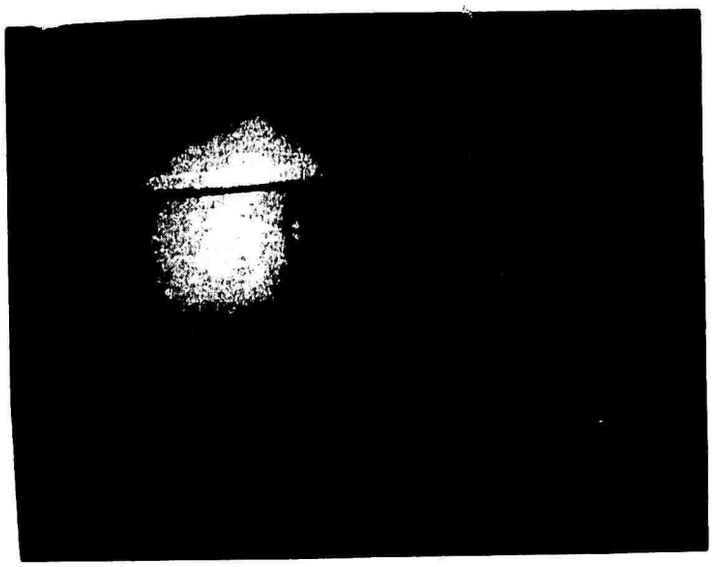

FIGURE 16

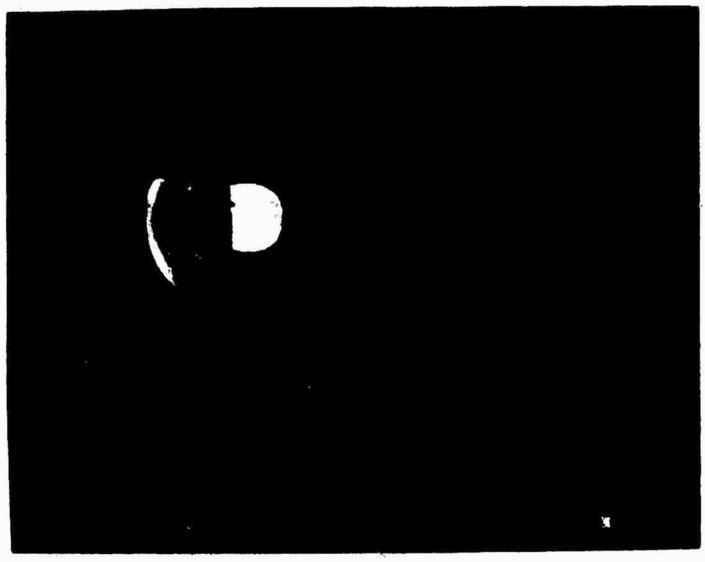

FIGURE 17

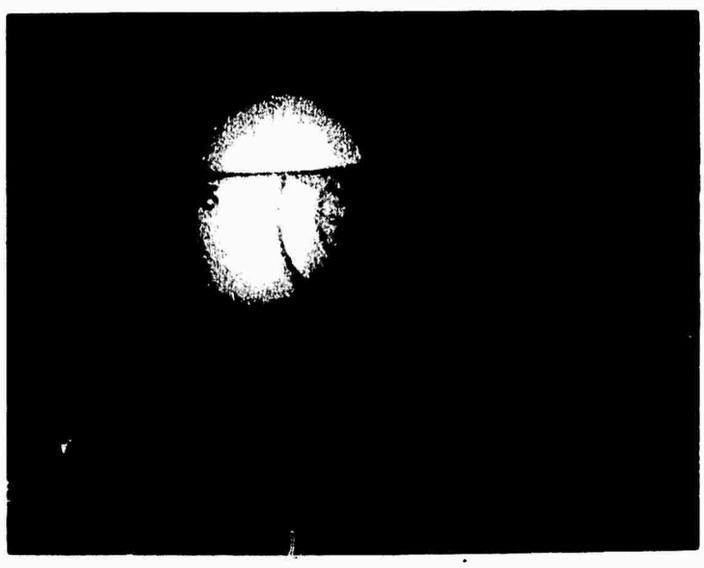

FIGURE 18

The internal energy for air has been calculated[6] to be

$$\epsilon \approx 2.7 \times 10^5 \, T^{3/2} \, (\rho/\rho_o)^{0.12} \text{ erg/gm}, \qquad (4)$$

where ρ/ρ_o is the density of air referred to standard conditions.

Using this as a rough approximation of the internal energy of the surface plasmas in these photos we obtain, with $\gamma = 1.2$,

$$T_i \approx 5.4 \times 10^{-4} \, V_T^{4/3}, \qquad (5)$$

where T_i is the ion temperature of the plasma.

Table 1 lists the average transverse velocities $\langle V_T \rangle$ obtained by measuring the expansion of the plasma between two times t_1 and t_2. That is,

$$\langle V_T \rangle = \frac{r_2 - r_1}{t_2 - t_1}, \qquad (6)$$

where r_2 is the radius of the plasma at time t_2 and r_1 the radius at t_1. The listed values of T_i are obtained from (5).

Table 1

Plasma Expansion Velocities and Ion Temperatures

t_1(ns)	t_2(ns)	$\langle V_T \rangle$ cm/sec	T_i °K
0	270	7.4×10^5	3×10^4
270	580	2.6×10^5	9×10^3
580	880	2.3×10^5	8×10^3
880	1600	1.5×10^5	4×10^3
1600	1900	1.4×10^5	4×10^3

Figures 19 and 20 are graphs of $\langle V_T \rangle$ and T_i respectively. The ion temperature is decreasing rapidly at 270 ns after the damaging pulse. It is undoubtedly much greater than 3×10^4°K in the inchoative plasma. Holograms taken with shorter delay times will yield a better value for T_i in this plasma.

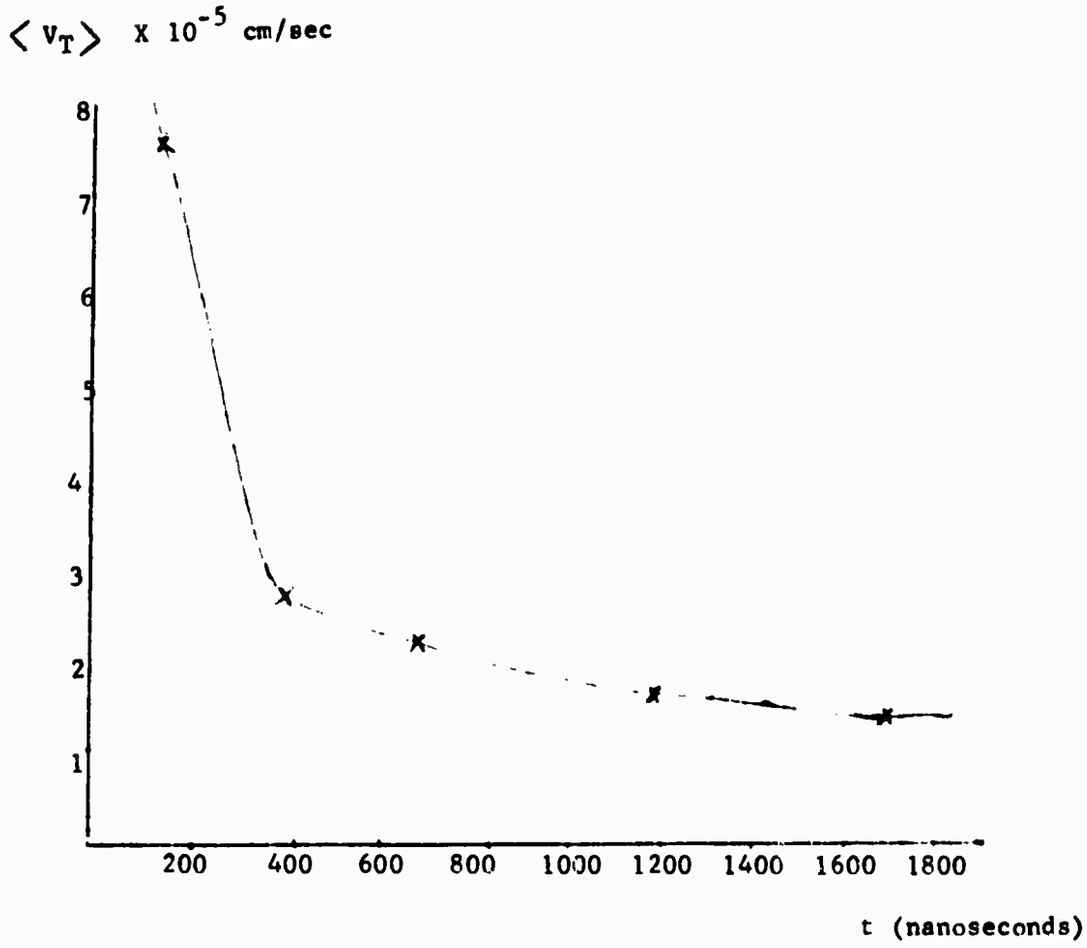

FIGURE 19 - $\langle V_T \rangle$ vs time

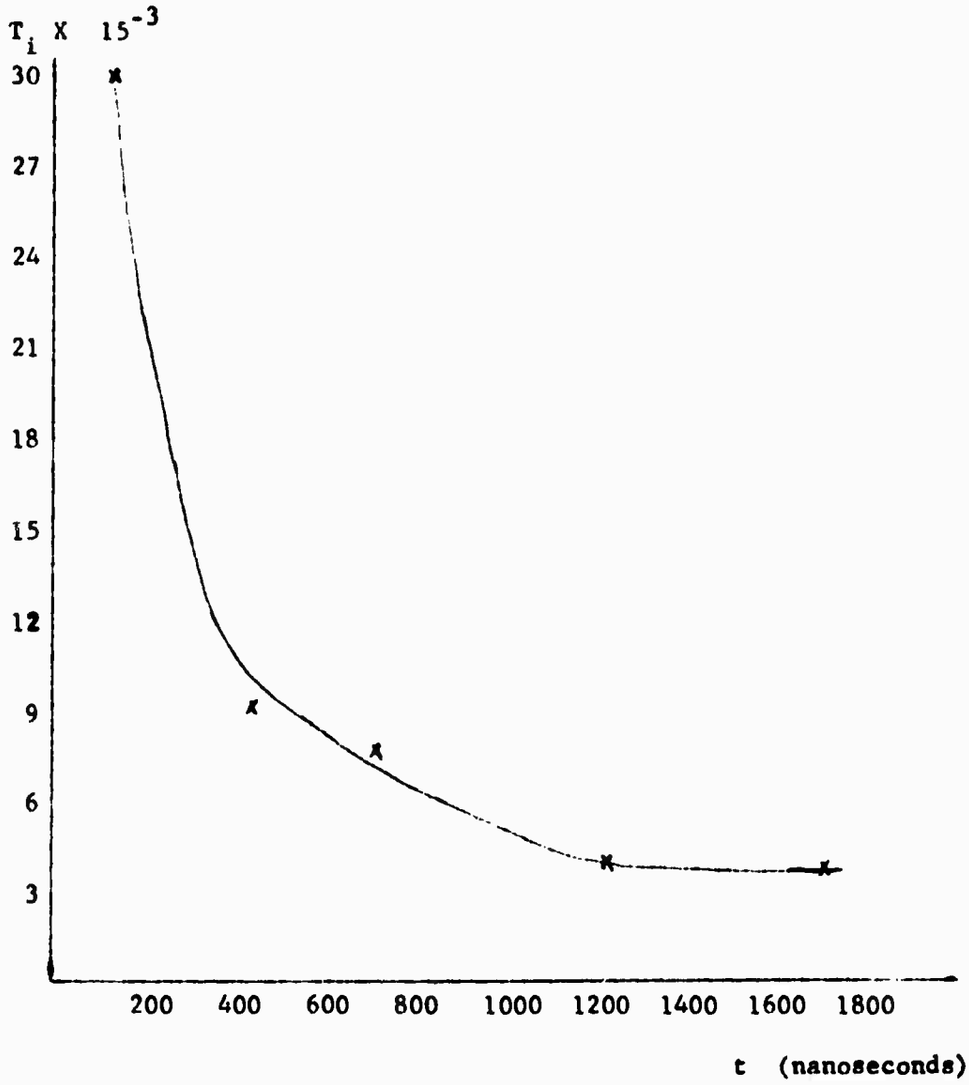

FIGURE 20 - T_i vs time

As a note of possible interest we remark in passing that these values of T_i are probably good values of the electron temperature also, since one expects the two species to reach equilibrium within a few nanoseconds in free plasmas of these densities.

Electron Densities in Surface Plasmas

To a good approximation, for the present purpose, the phase shift of the ruby laser light as it traverses the surface plasma is given by

$$\Delta\varphi = \frac{K_o}{2\, n_c} \int_o^d n(r)dr, \qquad (13)$$

where $\Delta\varphi$ is in radians, K_o is the wave number of ruby light, n (r) is the electron density at a distance r from the axis of the damaging laser beam, d is the transverse diameter of the plasma, and n_c is the "cutoff" electron density as given in equation 3.

Substituting for the known constants one obtains

$$\tau = 5 \times 10^{-23} \int_o^d n\,(r)\, dr, \qquad (14)$$

where τ is the number of fringes in the plasma, n (r) is electrons/m^2, and d and r are in meters.

Assuming now that n(r) is constant across the plasma, we obtain

$$n = \frac{2\,\tau\, 10^{18}}{d}, \qquad (15)$$

where n is now in electrons/cm^3 and d is in centimeters.

The assumption of constant n across the plasma will lead to a value of n(o) that is too small by a factor of perhaps 2, but the approximation is good enough for our purposes at the present time.

Applying (15) to the plasmas of Figure 2 we obtain, for both exit and entrance plasmas, $n \approx 2 \times 10^{19}/cm^3$. As mentioned above, the shot of Figure 2 was not far above the damage threshold, so this electron density should be representative of those encountered in damage to systems components.

In interpreting this number it must be remembered that the hologram of Figure 2 was taken after a time delay of 190 ns. Thus the plasma has expanded appreciably and it's density is much less than it was at the end of the damaging pulse. We can, however, obtain a "ballpark" number for the electron density of the plasma in its incipient stage. We assume that no recombination has occurred during the 190 ns delay. We also assume a reasonable value for the diameter of the plasma at the end of the damaging pulse. In this case this value is about 1 mm. Measuring the diameter of the plasma in the photo to be approximately 4 mm, and recognizing that the electron density goes as the inverse cube of the diameter, we obtain for the electron density of the inchoative plasma a value of $60 \times 2 \times 10^{19} = 1.2 \times 10^{21}/cm^3$. Considering the nature of the assumptions which have gone into this calculation, this number is undoubtedly low. The important point is that it is in the region where one expects the plasma to begin to absorb the damaging pulse. This is in keeping, as noted above, with observations made by other investigators.

2.4 Discussion and Conclusions

Although more extensive and well characterized experiments using the holographic technique presented herein need to be performed, a great deal of information can be gleaned from the work already done and some tentative conclusions can be drawn.

What is the evidence, in these holograms, for and against some of the theories which have been proposed to cause surface damage? Some of the points which can be made concerning this are enumerated below:

1.) In none of the holograms made thus far has any acoustic wave been detected moving toward the exit surface, except when there is gross internal damage of the sample. This indicates that any of the proposed mechanisms which postulate damage due to internally initiated acoustic disturbances are not valid.

2.) The hypothesis which holds that surface damage is caused by the shock of the expanding plasma takes cognizance of the fact that the plasma tends to grow into the laser pulse which creates it. This has been often observed and is quite reasonable since the plasma is being "fed" in the area facing the direction from which the laser pulse comes. This implies that the shock wave created by the expanding plasma also moves into the laser beam. (This has also been observed). At the exit, then, the shock strikes the surface, while at the entrance the shock moves away from the surface. This asymetry accounts for the difference in the nature of exit and entrance damage and the difference in damage thresholds.

Based upon this model it would be expected that strong acoustic disturbances would be seen at the exit but not at the entrance. A salient feature of the holograms in which damage occurred to the sample is that an

acoustic disturbance is almost always present at the exit face but is usually not seen at the entrance face. However, to conclude that exit surface pitting is caused by a shock wave from the expanding plasma would be a non sequitur. One would expect that acoustic waves of the sort observed would result from such a pitting. The question is "what causes the pitting?" This cause could be a mechanical shock or it could be a very rapid deposition of thermal energy. Thus the validity of neither the thermal erosion theory nor the mechanical shock theory is evinced by the acoustic disturbances seen in these holograms.

3.) In regards to the shock theory of surface damage, it is interesting to note (see Table 1) how close the velocity of sound in the plasma - that is, the transverse expansion velicity of the plasma - is to the velocity of sound in the glass. Remembering that the acoustic impedance of a solid is given by the product of the density of the solid and the speed of sound in the solid, and assuming that the density of the inchoative plasma is near that of the solid, it is seen that there is a good acoustic impedance match between the plasma and the glass sample. This would aid in coupling the plasma expansion shock wave into the glass.

4.) The opaque regions of the exit plasmas in many of the cases where pitting has occurred may be a clue to the mechanism operating to cause damage. If this opacity is due to material from the surface, then the material is being ejected at a high velocity. Measurements made in the photos of the holograms show that this velocity is in excess of 10^5 cm/sec. The implications of this are not clear to us at present.

5.) The acoustic waves seen emanting from interior damage tracks are potentially more conclusive than those from the surfaces. They are perhaps evidence that electrostriction is acting in at least some of the instances of self focusing observed in these holograms. One draws this conclusion from the fact that only a longitudinal wave is seen radiating away from internal damage tracks. If the breakage per se were causing the emission of the sound wave, then it might be expected that both longitudinal and transverse disturbances would be visible. However, electrostriction, which causes a radial constriction, would produce only a longitudinal wave. The evidence indicates, then, the existence of a relatively strong electrostrictive wave in some instances of self tracking damage. However, it must be stressed that this evidence is only preliminary.

We should note here that a sound wave is not always seen in conjunction with tracking damage. The shorter the time delay between damage and the taking of the hologram and the greater the tracking damage, the more likely it is that a wave will be seen. Perhaps the tracking wave is less intense than those from the exit face, and consequently, attenuates more rapidly to the point where it is not detected. Also, the holograms are not all of equal quality and it is likely that weaker disturbances are sometimes not detected because of poor quality of the hologram.

6.) The ion temperature of the plasma near the end of the damage pulse is probably much greater than 5×10^{4}°K. This supports the theory of thermal erosion. Also, the nature of the damage often suggests that it is

caused by high temperatures. There is often a large - sometimes as great as one centimeter in diameter when the energy density of the laser pulse is far above the damage threshold - area of permanent discoloration of the glass surface around the damage on the exit face. This diameter is much larger than the diameter of the damaging laser beam, but the plasma attains yet even larger dimensions. Furthermore, the ion temperature of the plasma can still be several thousand degrees upon reaching this diameter (see Table 1). There can be little doubt then that the plasma per se is responsible for this discoloration. Whether the mechanism responsible is thermal heating or UV radiadition from the plasma remains to be determined.

This large discolored area illustrates very well the point made earlier in this report concerning the efficacy of doing damage studies well above the damage threshold. Such a large area of discoloration would not be observed unless the energy density of the damage pulse is sufficiently great to cause a plasma of relatively large dimensions and, consequently, one would not be able to observe so easily the effect of the plasma on the glass.

7.) In general, any hypothesis whose purport is explanation of surface damage must take into account the great difference between entrance and exit surface damage thresholds. Most do this, but there appears to be another difference between exit and entrance damage which is not taken into account. The entrance and exit plasmas are of about the same density and temperature but the exit plasma is often much larger when the energy of the beam is well above the damage threshold. This asymetry could be an indication of the damage mechanism.

4.3 A Proposed Damage Mechanism *

In an effort to colligate the facts gleaned from these observations, we present the following phenomenological model as an explanation of surface damage.

At the exit surface a plasma is initially formed by desorption of impurities from the surface by the leading edge of the laser pulse. That impurities and not the glass per se are responsible for the plasma is evinced by the fact that pristine glass is quite difficult to damage. These impurities may be remnants of polishing compound, water absorbed from the atmosphere, etc. This desorption and plasma formation are enhanced by any self trapping of the beam which might occur. The plasma remains in close contract with the surface due to its propensity to grow into the laser beam. UV radiation from the plasma raises electrons in the surface to the conduction band until the surface begins to appear metallic to the still incident laser pulse. This in turn leads to an increased absorption of the pulse and, consequently, to an increased rate of plasma growth. The characteristic pit is due to either thermal spallation or to a combination of thermal effects and the shock from the expanding plasma acting upon the already thermally weakened surface. The larger area of discoloration around the pit is due to the thermal effect of the plasma or to UV radiation from the plasma.

* Some of the essentials of this must be credited to Prof. A. Glass of Wayne State University, Detroit, Michigan.

The entrance surface damage threshold is higher and the plasma smaller because the plasma grows away from the surface. Consequently, the entrance is not as effectively subjected to either radiation or shock from the plasma. Any entrance damage is due to thermal effects,

A possible point of contention in this proposed mechanism lies in the rather blasé statement that the entrance surface is not as effectively irradiated by UV from the plasma as the exit surface. At present, nothing more than the observation that there is greater contiguity between exit and plasma than between the entrance and plasma can be offered. This is certainly a point that wants more thought.

3. TEM_{00} MODE LASER

As reported in the semi-annual report of 31 December, 1970, a high power, high energy, laser operating the TEM_{00} spatial mode is being designed and constructed under this contract. This will be a glass oscillator-amplifier system with a pulse width variable from approximately two to forty nanoseconds.

Since the building of this laser is still a process, only the oscillator design will be discussed herein. The complete system will be described in the next semi-annual report, due 31 December 31, 1971.

Several problems have presented themselves in the design of this oscillator. Some of these problems, along with pertinent comments, are as follows:

1.) Characteristics of the TEM_{00} mode - Ideally the output of an oscillator operating in the TEM_{00} mode should process a Gaussian cross-section. That the output is spatially Gaussian can be ostensibly verified by several methods. Two common ones are examination of the burn patterns of the laser (the laser is fired through filters of various neutral densities and is assumed to have a reproducible output) and measurement of the energies passing through apertures of various sizes.

These two methods examine only the time integrated output of the laser. McAllister, et. al., have shown that a more complete examination of the laser pulse must be made. Specifically, the temporal shape of the pulse as a function of radial distance from the axis of symmetry must be determined. This shape should be the same for every point in the cross-section of the pulse if "TEM_{00}" is to have its usually inferred meaning. In other words, the spatial cross-section of the pulse must be Gaussian along the whole length of the pulse.

These conditions are only approximately fulfilled in practice. The pulse is never truly Gaussian in a laser which uses an intensity aperture and there is always picosecond structure to the pulse. However, the conditions can be well approximated in the nanosecond regime.

In the oscillator under consideration here (Figure 21), there appears to be no problem with variation in time of the cross-sectional shape of pulse. This has been checked by passing a portion of the beam through a pinhole located at various positions in the beam. However, unless care is taken a great deal of longitudinal mode beating is present in the output. Figures 22, 23, and 24 are oscillograms of the entire pulse for cavity lengths of 5, 2 and 1 meters respectively. The time scale is 20 ns/division in each Figure. That the regular pattern is due to mode beating can be ascertained by noting that the frequency is $\frac{2c}{l}$. As the frequency separation of the modes varies as $\frac{1}{l}$, the problem largely disappears with the one meter cavity. (It is interesting to note in these oscillograms that the temporal pulse width is directly proportional to the cavity length).

FIGURE 21 - Oscillator

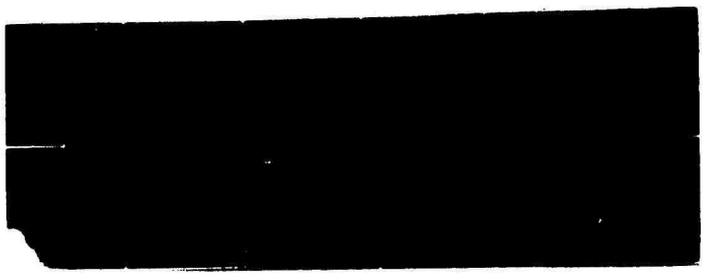

FIGURE 22

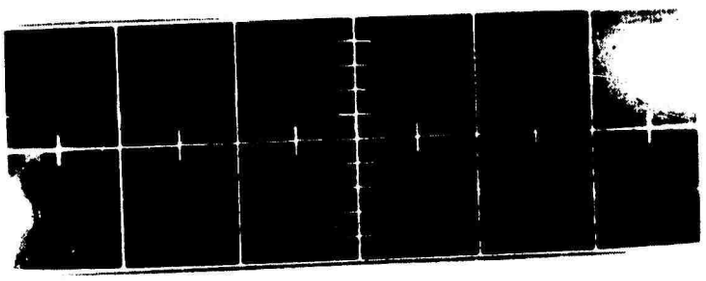

FIGURE 23

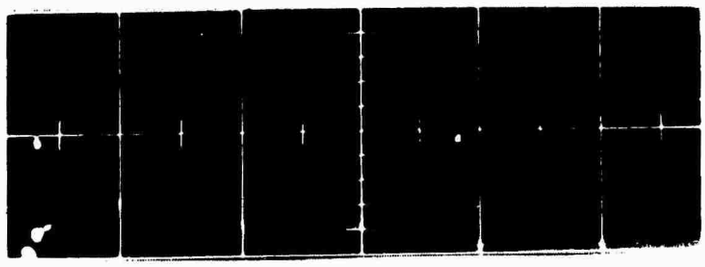

FIGURE 24

Another aspect of TEM_{oo} mode characterization is the spatial "cleanliness" of the pulse. There is always some energy outside the burn pattern which seems to define the beam. This is often not manifested until attempts to amplify the pulse are made. The amplification of this peripheral energy can result in a very messy looking beam. Generally the problem lies in scattering from the intercavity aperture used to obtain the TEM_{oo} mode. Special apertures can be used to alleviate this problem and such an aperture has been installed in the oscillater described here. The efficacy of this remains to be seen after the pulse is substantially amplified.

2.) Obtaining the TEM_{oo} mode - We have used the most straightforward method to this end, an aperture placed inside the oscillater cavity. Besides use of an aperture, several other factors govern the ease with which the mode can be obtained and the maximum size aperture that can be used:

a.) The optical quality of the intercavity elements must be "good". Upon the first attempt to run the oscillater under consideration in the TEM_{oo} mode, we used a laser rod which exhibited a full wave (full aperture) of stress when examined in a Michelson interferometer. The TEM_{oo} mode could not be obtained even with an aperture as small as 0.5 mm in diameter. Replacement of this rod with one with less than 1/5 wave stress led immediately to operation in the desired mode.

Cleanliness of the optical elements is, of course, of paramount importance not only for maintenance of optical quality but also for the prevention of damage.

b.) Any small damage site which develops in the path of the beam inside the oscillator cavity can cause loss of the TEMoo mode. This is often manifested by the sudden appearance of a higher order mode.

c.) The use of a curved mirror renders attainment of the TEMoo easier. A four meter radius of curvature mirror is being utilized in our oscillator as a rear reflector. The output mirror is an Ekalon with an infinite radius of curvature.

d.) Alignment of the cavity is critical, not only for circular symmetry of the output beam but also for attainment and maintenance of the mode desired. As a general procedure we align the cavity to lase and then "play" with the aperture and front mirror to obtain the best appearing burn pattern.

e.) It should be mentioned that a 19mm diameter rod is utilized in this oscillator, but only a three millimeter section near the center is selected by the aperture as the lasing region. This might affect the results we are obtaining, since the thermal profile would be different for a smaller rod.

3.) Ascertainment of the presence of the TEM_{oo} mode -

The evidence we have for TEM_{oo} operation is fourfold:

a.) The burn pattern, in the near and far fields, shows the correct profile when taken through various neutral density filters.

b.) The presence of a higher order mode manifests itself quite obviously in the burn pattern if the mode selecting aperture used is too large or, often, if a damage site occurs in one of the optical components in the cavity. This obvious shifting from mode to mode is conclusive evidence that the laser is operating in a single spatial mode.

c.) The output beam exhibits spatial coherency across its' entire cross-section. This is evidenced by the observation of a relatively large hole in the burn pattern after the beam has passed through an amplifier rod with an inclusion in the path of the beam. The inclusion leads to pronounced diffraction effects in the single mode case, but does not manifest itself at all in the burn pattern when the laser is operating multimode.

d.) The output beam is temporally satisfactory across its complete cross-section.

4.) Energy extractable from oscillator - The amount of energy obtainable from this oscillator is, for an aperture of given diameter, limited not by the lasing quality of the rod, but by the damage threshold of the intercavity elements. We have been able to obtain as much as 800mj, using a 3mm aperture, in the TEM_{oo} mode. This, however, rendered the intercavity power density far above the damage threshold of the optics.

Hence the final design of the oscillator will be such that the intercavity power density will never exceed 0.5 gigawatts/cm^2 at any time or position. This means that the temporal and spatial shape of the output pulse must be taken into account when peak intercavity power densities are calculated. We have used, as an acceptable approximation, a factor of 2 in both the temporal and spatial cases in calculating peak power densities inside the cavity. That is, the peak power density is considered to be approximately four times as great as that calculated from a consideration of the average power densities in space and time. Since the intercavity power density at the output mirror, where it is greatest, is related to the output power density as

$$P_{in} = P_{out} \frac{R + 1}{R - 1} ,$$

where R is the reflectivity of the output mirror, and since we are utilizing a mirror with a reflectivity of 28%, we can conclude that the average output power density must be no more than approximately one eighth of damage threshold if the intercavity elements are to have a long lifetime without damage. This means, then, that power densities of slightly less than 100 megawatts/cm^2 can be safely extracted from the oscillator.

Considering the high gain per pass achievable with the 9" of pumped rod in this oscillator, it is possible that the reflectivity of the output mirror can be reduced and, consequently, the amount of energy extractable from the oscillator increased. This will be investigated.

The most damage prone elements in the cavity have proven to be the Brewster stack glass polarizers, and the KD*P crystal in the Pockels cell. The laser rod does not damage anywhere near as easily as any of these. It is possible that polarizers made of ED-4, which is the same material as the laser rod except that it contains no Neodymium, will improve the situation and allow operation at higher power densities.

One might conclude that since the energy out of the oscillator must be limited due to the possibility of damage, a shorter laser rod could be used. We have attempted to use a shorter rod, 4" of which was pumped. The result was that the gain was not sufficient to produce lasing action without relatively hard pumping. This leads to thermal problems and makes the TEMoo mode more difficult to achieve and maintain. In an oscillator of this kind, it seems best to use a longer rod than one might think necessary from an energy standpoint.

Another factor which appears to affect the energy of the oscillator, at a given pumping level and with an aperture of given size, is the geometry of the aperture. In an effort to keep the output cleaner, we have been using a metal disk with the aperture in it at the end of a truncated cone. Figure 25 shows this geometry. The inside of the cone is bright metal. Using this aperture, as opposed to one formed by simply drilling a cylindrical hole through a disk, the output of the oscillator is approximately 30% higher at a given pumping level. A reasonable explanation for this is that scattering from around the cylindrical aperture is depleting the upper lasing level through off axis photons scattered through the lasing volume.

FIGURE 25 - Cross section of Intercavity Aperture

The oscillator for the damage study laser, then, is essentially complete. Only some optimization remains to be done. It is expected that 200-300 millijoules will be obtained in a 20-40ns pulse. This will be in the TEM_{oo} mode with a well behaved temporal profile across the entire beam.

Plans for the near future call for the installation of an optical shutter to obtain pulses as short as two or three nanoseconds. Besides this, of course, the amplifier chain will be assembled and the final beam characterized. All of this should be achieved within the next two to three months.

PRACTICAL APPLICATION OF THERMODYNAMICS TO LASER GLASS MELTING

4.1 INTRODUCTION

Platinum inclusions in laser glass appear to be caused by migration of Pt as platinum oxide. Gas phase transport is possible with PtO_2(gas) being the major intermediate species; whiskers and platelets are expected morphologies. Transport through the glass as a platinum oxide complex may also be possible.

The Pt metal can be stabilized with respect to its oxide by reducing a partial pressure of O_2 (P_{O_2}). In stabilizing the Pt metal, the oxides in the glass melt are destabilized in favor of their metals resulting in the formation of Pt alloys. The following reactions illustrate this problem.

$$Pt(\text{pure metal}) + O_2(\text{gas}) \rightarrow PtO_2(\text{gas}) \qquad (1)$$

$$Si\ (\text{in solid Pt alloy}) + O_2(\text{gas}) \rightarrow SiO_2\ (\text{in laser glass melt}) \qquad (2)$$

As the P_{O_2} is reduced, both Si and Pt are stabilized with respect to their oxides. It is apparent that the P_{O_2} must be chosen so that the P_{PtO_2} is as low as possible without the laser melt oxides reducing to the metal and attacking the Pt crucible. In order to determine the P_{O_2} at which all glass components react with Pt in a detrimental way, the standard state free energy for Reaction (1) and those for reactions similar to Reaction (2) for all oxides in laser glass, the thermodynamic activities of the various oxides in laser glass, and the thermodynamic activities of the corresponding metals in platinum must be known.

The standard state free energy of Reaction (1) has been determined by Alcock and Cooper[1]. The standard state free energy for the formation of the common oxides $\left[\Delta F_f^\circ(MeO_x)\right]$ have also been determined[2]. The ΔF°'s correspond to the energy difference between reactants and products when the solids and liquids are pure and when the gases are at 1 atm. of pressure. The thermodynamic activities yet to be determined take into account that the oxides are in a glass solution and that the metals are in the platinum alloy. The desired activities are not available from past scientific studies. The goal of this effort, therefore, is to determine the activities of oxides in laser glass and the activities of the metals of the laser glass in platinum.

During the 1971 fiscal year, emphasis has been placed upon (1) a literature search; (2) the estimation and (3) the experimental determination of the activities of oxides in laser glass and of metals in platinum.

The main emphasis of the 1972 fiscal year is to reduce to practice the concept of melting laser glass under reduced oxygen partial pressures in order to eliminate Pt inclusions.

4.2 LITERATURE SEARCH

The Semi-Annual Technical Report[3] submitted on January 1, 1971 contains the bulk of the literature search on thermodynamic activities. Appendix I of this report adds additional references not listed previously. Appendix I is divided into the same headings used in the semi-annual report:

1. Activities of Oxides in Binary and Ternary Systems;
2. Activities of Metals in Platinum
3. General Data on Similar Systems and Methods of Estimating Thermodynamic Activities, Free Energies of Formation, and Heats of Formation.

This is the first attempt of gathering and consolidating activities of oxides and of platinum alloys to appear in a literature. Several data banks and individual authors have contributed to the bibliography.

4.3 DETERMINATION OF ACTIVITIES

A. Empirical Study

For the literature search several glass compositions were considered, as presented in Table 2. The empirical determination of activities was narrowed to one glass composition, composition #5 in Table 2, a Li_2O-CaO-SiO_2-Nd_2O_3 glass.

The analytical technique which was developed and used at Battelle was particularly applicable to the overall project. Basically, the analytical technique consisted of equilibrating the laser glass with a small piece of platinum. After the equilibration, the platinum was placed in a Knudsen cell and the activities of the various metals from the laser glass picked up by the platinum were measured. Since the platinum had been equilibrated with the laser glass and since the free energies of formation of the oxides have been previously determined[2], the activities of these oxides in the laser glass could be calculated. The details of the analytical technique are described in Appendix II.

There are two basic advantages to the analytical technique. First, with a minimum amount of experimentation and time, activities were determined in the platinum and in the laser glass. Second, several oxide activities were determined; direct measure of the oxide activities by placing the glass directly into the Knudsen cell would have given only the oxide activity related to the most volatile species, probably only Li_2O.

TABLE 2

LASER GLASS COMPOSITIONS OF COMMERCIAL INTEREST

Glass No.	Component	Mole Fraction
1	SiO_2	0.785
	BaO	0.014
	Na_2O	0.080
	K_2O	0.112
	Nd_2O_3	0.010
2	SiO_2	0.719
	Al_2O_3	0.014
	Sb_2O_3	0.002
	BaO	0.014
	ZnO	0.017
	Li_2O	0.023
	Na_2O	0.068
	K_2O	0.113
	Nd_2O_3	0.010
3	SiO_2	0.791
	TiO_2	0.004
	Sb_2O_3	0.005
	BaO	0.018
	PbO	0.006
	Na_2O	0.045
	K_2O	0.126
	Nd_2O_3	0.006

TABLE 2
LASER GLASS COMPOSITIONS OF COMMERCIAL INTEREST (cont'd)

Glass No.	Component	Mole Fraction
4	SiO_2	0.480
	B_2O_3	0.174
	Al_2O_3	0.073
	As_2O_3	0.073
	BaO	0.255
	Nd_2O_3	0.013
5	SiO_2	0.593
	Al_2O_3	0.025
	K_2O	2.12×10^{-7}
	CeO_2	1.6×10^{-3}
	Fe_2O_3	9.4×10^{-8}
	Na_2O	9.42×10^{-7}
	Li_2O	0.275
	Nd_2O_3	0.005
	CaO	0.100
6	SiO_2	0.762
	Al_2O_3	0.017
	Sb_2O_3	0.002
	BaO	0.023
	ZnO	0.017
	Li_2O	0.023
	Na_2O	0.077
	K_2O	0.080
	Nd_2O_3	0.010

TABLE 2
LASER GLASS COMPOSITIONS OF COMMERCIAL INTEREST (cont'd)

Glass No.	Component	Mole Fraction
7	SiO_2	0.792
	Al_2O_3	0.010
	BaO	0.022
	ZnO	0.012
	Li_2O	0.022
	Na_2O	0.080
	K_2O	0.053
	Nd_2O_3	0.007
8	SiO_2	0.773
	Sb_2O_3	0.002
	BaO	0.113
	Na_2O	0.100
	K_2O	0.013

B. Results of Empirical Study

The determined activities are presented in Table 3.

The activity of aluminum in platinum (A_{Al}^{Pt}) is given at 2300°K because insufficient data were available to empirically extrapolate to the desired 1700°K.

The $A_{Al_2O_3}^{glass}$ @1700°K cannot be calculated without an estimate of A_{Al}^{Pt} @1700°K because the long term equilibration was carried out at this temperature. As the partial pressure of oxygen is reduced, the activities of the metals in platinum (A_{Me}^{Pt}) increases as their mole fractions in platinum (X_{Me}^{Pt}) increase which is expected. From the relation: $A_{Me}^{Pt} = \gamma_{Me}^{Pt} \times X_{Me}^{Pt}$, the activity coefficient of the various metals in platinum (γ_{Me}^{Pt}) can be calculated. They are presented in Table 4. In general, several metallic systems follow Henry'sLaw; that is, the activity coefficient is not a functionof composition in dilute solutions. From Table 4, however, it can be seen that the activity coefficient of one of the important metals, silicon, is varying significantly with the partial pressure of oxygen. Extrapolation of the activity data to other compositions will be more difficult. The activity coefficient of the other metals in platinum do not appear to be strong functions of composition in the dilute solution range.

The activities of the oxides in the laser glass are not varying significantly with the partial pressure of oxygen as indicated in Table 3. This is to be expected because the composition of the laser glass equilibrated with the platinum at the various partial pressures of oxygen has not changed composition.

TABLE 3

EXPERIMENTALLY DETERMINED ACTIVITIES OF COMPONENTS IN PLATINUM AND IN GLASS AT EQUILIBRIUM AT 1700°K

Activities (A_{Me}^{Pt}) and Mole Fractions (X_{Me}^{Pt}) of Metals in Platinum:

	P_{O_2} (atm) during Equilibration		
	10^{-6}	10^{-8}	10^{-10}
A_{Si}^{Pt}	6×10^{-14}	5.5×10^{-12}	3×10^{-10}
X_{Si}^{Pt}	8.6×10^{-5}	2.8×10^{-4}	3.3×10^{-4}
A_{Li}^{Pt}	10^{-9}	10^{-8}	2×10^{-8}
X_{Li}^{Pt}	5×10^{-5}	2.5×10^{-4}	4.0×10^{-4}
A_{Al}^{Pt}@2300°K	2×10^{-7}	1.4×10^{-6}	1.1×10^{-5}
X_{Al}^{Pt}	3.3×10^{-5}	4.7×10^{-5}	1.5×10^{-4}
A_{Ca}^{Pt}	--	2×10^{-10}	9×10^{-11}
X_{Ca}^{Pt}	--	4.0×10^{-5}	9×10^{-5}

TABLE 3 (Cont'd)

EXPERIMENTALLY DETERMINED ACTIVITIES OF COMPONENTS IN PLATINUM AND IN GLASS AT EQUILIBRIUM AT 1700°K

Activities ($A^{glass}_{MeO_x}$) and Mole Fractions ($X^{glass}_{MeO_x}$) of Oxides in Glass:

	P_{O_2} (atm) during Equilibration		
	10^{-6}	10^{-8}	10^{-10}
$A^{glass}_{SiO_2}$	0.3	0.28	0.15
$X^{glass}_{SiO_2}$	0.593	0.593	0.593
$A^{glass}_{Li_2O}$	10^{-11}	10^{-9}	6×10^{-10}
$X^{glass}_{Li_2O}$	0.275	0.275	0.275
$X^{glass}_{Al_2O_3}$	0.025	0.025	0.025
A^{glass}_{CaO}	--	1.	0.1
X^{glass}_{CaO}	0.100	0.100	0.100

TABLE 4

ACTIVITY COEFFICIENTS FOR CONSTITUENTS IN PLATINUM

Element	P_{O_2} for Equilibrium		
	10^{-6}	10^{-8}	10^{-10}
Si	7×10^{-10}	2×10^{-8}	9×10^{-7}
Li	2×10^{-5}	4×10^{-5}	5×10^{-5}
Al	6×10^{-3}	3×10^{-2}	7×10^{-2}
Ca	--	5×10^{-6}	1×10^{-6}

4.4 ESTIMATES BASED UPON THEORETICAL MODELS COMPARED TO OBSERVED DATA

Now that activity data are available for the platinum and oxide systems of interest, the theoretical models for estimating thermodynamic data reported in the Semi-Annual Technical Report[3] of 1 January 1971 can be tested.

A. Motts Emissibility Criterion

A method of estimating the heat of formation of various metallic compounds $\left[\Delta H_f^{\circ}(AB_n)\right]$ was attempted from B. W. Motts' emissibility criterion. The estimations of several metallic compounds were not found to be successful. Actually this is not surprising. The Mott expression for the heat of formation is the sum of the heat of formation used in the Pauling model and the heat of formation used in the Hildebrand model. Both models by themselves estimate the heat of formation quite well for the particular classes of compounds for which they were developed; Pauling's model works well for ionic and covalent bonded compounds and Hildebrand's model works well for emmissible, molecular solutions. Isolated successes have been obtained by applying these models to metallic systems. By adding the heat of formation from the two models, however, one obtains an expression which is redundant; adding the two models together is not the same as applying a correction factor to one of the models[4]. As an example, consider one model giving an estimate of $\Delta H_f^{\circ}(AB_n) = -40$ kilocallories per mole and some other model giving an estimate of $\Delta H_f^{\circ}(AB_n) =$ 50 kilocallories per mole. It would not be appropriate to combine the two models and estimate the $\Delta H_f^{\circ}(AB_n)$ to be -90 kilocallories per mole. B.W. Mott may have found his expression appropriate for determining whether or not a metallic system is going to be immissible, but it is not an appropriate model for determining a heat of formation of metallic compounds.

B. Electronegativity

The Semi-Annual Report[3] indicated that when more reliable data were available from the empirical Battelle study, Pauling's electronegativity scale could possibly be re-evaluated for the platinides. If Li, Ca, Al, and Si are considered to be the same family of compounds, one could evaluate a new value for the electronegativity of platinum (E_{Pt}) which may be more appropriate for the platinides of interest. If the electronegativity of platinum is constant for these alloys, one may also expect the electronegativity of platinum to be constant for the other metals of interest, such as Na, K, and Mg. Instead of using a heat of formation $\left[\Delta H_f^\circ\ (MePt_x)\right]$ it was suggested that the excess molar free energy in the limit of the dilute solution $\left[F_{Me}^{-xs} = -RT \ln \gamma_{Me}^{PT}\ (\text{in Pt soln}, \lim X_{Me} \rightarrow \bar{0}) \approx H_{Me}^{-xs}\right]$ may be more appropriate. Such a term removes the compositional variance of activity; F_{Me}^{-xs} is similar to a $\Delta H_f^\circ\ (MePt_x)$ except that the compositional dependence has been removed. If it is assumed that the activity coefficient in the dilute range are composition independent, the excess free energies can be calculated from Table 4 and used in the Pauling equation in order to determine an electronegativity value for platinum (E_{Pt}). Table 4 lists the data used in the calculation. Column 1 lists the metallic element of interest. Column 2 lists the Pauling electronegativity[5] of the corresponding element. Column 4 lists the number of valence electrons (n). Column 5 is the calculated platinum electronegativity using the Pauling equation: $\Delta H_f^\circ\ (AB_n) = -n\ (23060)\ (E_a - E_b)^2$. Because the electronegativity for platinum (E_{Pt}) does vary significantly, using the

TABLE 5
CALCULATION OF A REVISED VALUE FOR
THE ELECTRONEGATIVITY OF Pt

Metal Element	E_{Me}^{5}	γ_{Me}^{Pt} ($\lim X_{Me}^{Pt} \to 0$) From Table	n	$E_{Pt} = E_{Me} - \left[\frac{-RT \ln \gamma_{Me}^{Pt}}{23,060\ n}\right]^{1/2}$
Li	1.0	4×10^{-5}	1	2.22
Cu	1.0	5×10^{-6}	2	1.95
Al	1.5	3×10^{-2}	3	1.91
Si	1.90	2×10^{-8}	4	2.71

Pauling electronegativity expression in order to calculate heats of formation (ΔH_f° ($MePt_x$), excess free energies ($\bar{F}_{Me}^{xs}$), or activity coefficients (γ_{Me}^{Pt}) for other metals of interest in platinum would not be accurate to within 2 orders of magnitude. Note that the electronegativity of platinum does not appear to be due to the choice of n values.

The experimentally determined activities of the oxides in the laser glass composition #5 are compared to the estimates made in the Semi-Annual Report[3] in Table 6. The method of estimating the activities of oxides is not satisfactory if the activities are desired within two orders of magnitude.

TABLE 6

COMPARISON BETWEEN OBSERVED AND ESTIMATED ACTIVITIES OF OXIDES

	A_{MeO_x}	
Oxide	Observed	Estimated
Li_2O	10^{-9} to 10^{-11}	6×10^{-6}
CaO	1 to 0.1	8×10^{-3}
SiO_2	0.3 - 0.15	0.37

4.5 MORPHOLOGIES OF PLATINUM INCLUSIONS

Platinum inclusions have been found to occur as four different types of morphologies. Whiskers and platelets (such as triangles and polygons) have usually been attributed to the vapor phase growth of the inclusions. Figure 26 compares a local devitrification (left) to a platinum whisker surrounded by some devitrification. Lacy networks and agglomerates have been attributed to precipitation from solid solution; they may also be caused by localized heating of the Pt crucible when an induction furnace is used.

Photomicrographs of the glass samples used in the equilibration and determination of activities at Battelle are shown in Figure 27. Initially the glass was made from batch in a nitrogen atmosphere for 24 hours. Microscopic examination indicated that no platinum inclusions were present after this heating. The total Pt content was analyzed and found to be approximately 1.5 ppma. The glass sample was then equilibrated for 168 hours at the various partial pressures of oxygen used in the study:

$$P_{O_2} = 10^{-9}, 10^{-8} \text{ and } 10^{-10} \text{ atm.}$$

The total platinum content was analyzed again and found to be approximately 0.6 ppma.

The decrease in total Pt content of the glass from 1.5 to 0.6 ppma may have been caused by one of the Pt in the glass precipitating on the Pt crucible and submerged wire in the long term equilibration; since a small sample size was used the surface to volume ratio was high. The 1.5 ppma was obtained by fire assay on a 30 g. sample while the 0.6 ppma was obtained

FIGURE 26 - INCLUSIONS IN PRODUCTION LASER GLASS

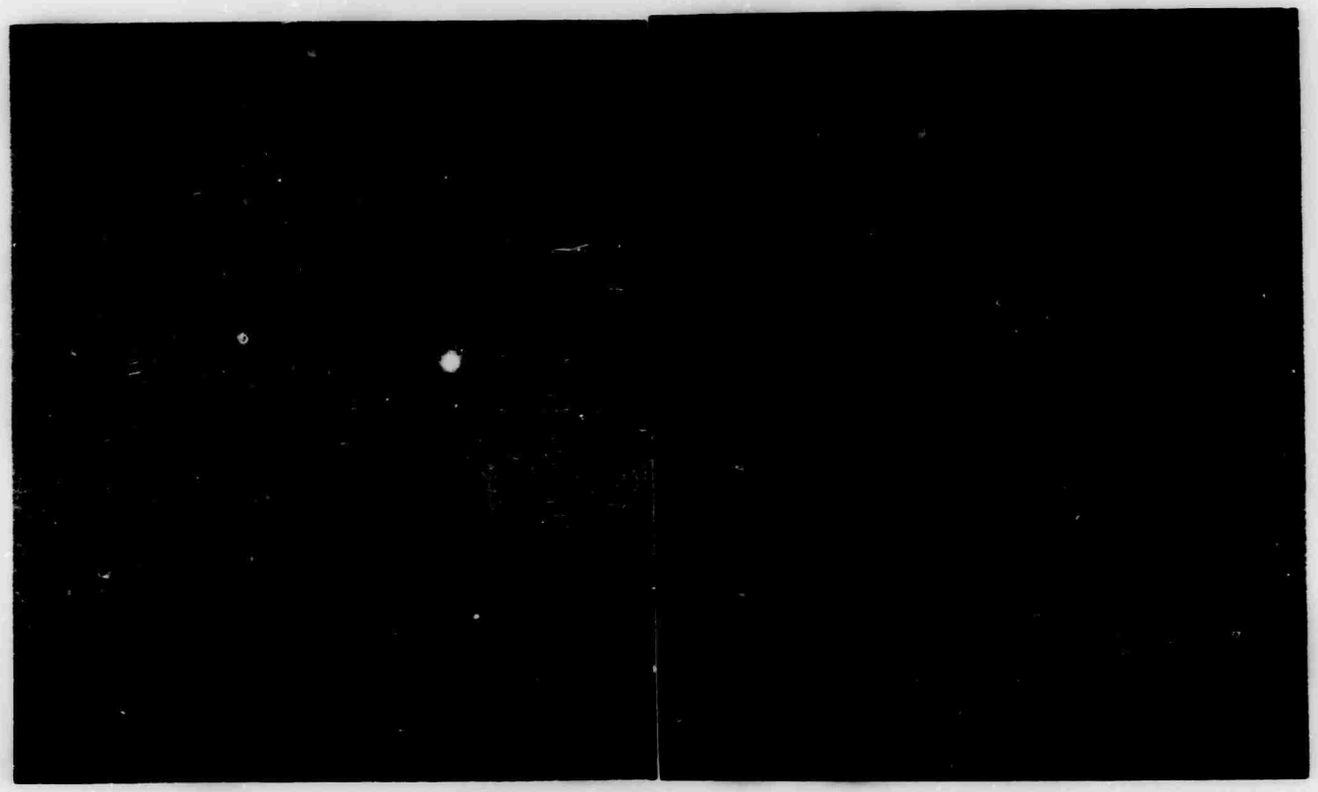

FIGURE 27 - Pt SPARKLER EFFECT IN LASER GLASS MELTED AT $P_{O_2} = 10^{-10}$ atm.

with a Knudsen Cell-Mass Spectrometer on a less than one gram sample. The difference in sample size and the difference in analytical methods may also account for the observed difference. Microscopic examination of the glass showed a new type of inclusion best described as a "salt effect". Figure 27 is representative of the samples used in the long term equilibration. The low magnification photomicrograph on the left shows the large number of inclusions and the photomicrograph on the right shows the very small size of the inclusions. (The bright spot in the low power micrograph is a surface defect, out of focus, and not the "salt" effect discussed).

It is believed that this type of inclusion is more representative of platinum dissolution and precipitation from solution. It may also indicate that Pt can be precipitated from a glass heated in a relatively oxygen deficient atmosphere, such as N_2, by exposing the glass to a more reducing atmosphere. At any rate, the P_{O_2} is a significant parameter related to the occurrance of platinum inclusions in laser glass.

4.6 PLATINUM FAILURE VS. P_{O_2}

The purpose of gathering thermodynamic data and experimentally determining the activities of the oxides in glass and of the corresponding metals in platinum was to predict the point of "failure" of the platinum parts in contact with the glass during the melting operation. Now that the data for glass composition #5 have been determined, the lowest oxygen partial pressure one can use for melting glass composition #5 in platinum without failing the platinum can be predicted. It is desired to reduce the partial pressure of oxygen as low as possible in order to minimize the partial pressure of PtO_2 (gas) above the melt and the activity of the corresponding platinum oxide complex in the glass. The lower limit is set by platinum failure.

What is meant by platinum "failure"? Failure would occur: (1) if a liquid phase was formed; (2) if an intermetallic compound formed; or (3) if a large increase in the Pt lattice parameter (d spacing) occurred on addition of metal contamination. Most of the metal-platinum phase diagrams of interest are not available. For those which are available, $\sim$ 1 at .% of the metal in platinum can be dissolved before failure would be expected.

The details of the thermodynamic calculations in order to estimate the partial pressure of oxygen required for platinum failure are presented in Appendix III. The results of the calculation are

presented in Table 7. The first column lists the metal in platinum solution expected to cause the failure. The second column lists the partial pressure of oxygen required for failure.

Platinum failure is expected to occur by silicon attack somewhere below 10^{-11} atm. and possibly not until 10^{-13} atm. at 1700°K (2600°F). The lithium, aluminum and calcium are not expected to cause the platinum metal failure until a lower P_{O_2} is reached within the glass.

From the equilibration studies, it was experimentally determined that laser glass could be melted in platinum at an oxygen partial pressure of 10^{-10} atms. at 1700°K without experiencing failure. The low partial pressure of oxygen for this run was chosen based upon the two previous equilibration runs.

During the next fiscal year, a small scale crucible melting program is planned to melt glass composition #5 in platinum at partial pressures of oxygen in the 10^{-10} atms. range and study the effect of the oxygen partial pressure on the platinum inclusions and life of platinum parts.

TABLE 7

ESTIMATED P_{O_2}'s BELOW WHICH Pt FAILURE IS EXPECTED

FROM THE VARIOUS GLASS CONSTITUENTS OF COMPOSITION #5 IN TABLE #2

Element	P_{O_2}
Si	10^{-11} to 10^{-13} atm.
Li	10^{-14} atm.
Ca	10^{-21} atm.

4.7 SUMMARY

1. Both theoretical considerations and a change in the P_{O_2} during the melting history of the samples used in the Battelle study indicate that the partial pressure of oxygen is an important parameter to control.

2. An extensive literature search has been compiled on the activities of metals in platinum and on the activities of oxides in glass.

3. Using various theoretical models, the thermodynamic activities of metals in platinum and of oxides in laser glass cannot be estimated within two orders of magnitude.

4. A technique was developed which enables the simultaneous determination of the activities of several oxides in a glass composition and the activities of corresponding metals in solution of one of the more precious metals, such as Pt, Pd, Rh, and Ir.

5. The thermodynamic activities of Li_2O, CaO, Al_2O_3, and SiO_2, have been determined in a Li_2O-CaO-SiO_2-Nd_2O_3 laser glass at 3 P_{O_2}'s. The activities of the corresponding metals in platinum have also been determined.

6. It has experimentally been determined that the Li_2O-CaO-SiO_2-Nd_2O_3 laser glass can be melted in platinum at an oxygen partial pressure of 10^{-10} atms. without crucible attack. Using the derived thermodynamic data it appears that oxygen partial pressures below 10^{-13} atm. would cause platinum crucible failure at 1700°K (2600°F).

REFERENCES

1. Alcock, C.B., and Hooper, G.W., "Thermodynamics of the Gaseous Oxides of the Platinum-Group Metals", Royal Society Proc. 254 (1960) 551-561.

2. JANAF Tables, Joint Army-Navy-Air Force Thermochemical Panel; JANAF Interim Thermochemical Tables, prepared by The Dow Chemical Company, Midland, Michigan, 1960 plus supplements.

3. Boling, N.L., Spanoudis, L., and Wengert, P.R., "Damage Threshold Studies of Glass Laser Materials", Semi-Annual Technical Report, December 31, 1971, Contract No. DAHC-15-69-C-0303.

4. Communication with Wayne L. Worrell, University of Penna., Philadelphia, Pennsylvania, July 8, 1971.

5. Pauling, Linus, "General Chemistry", W.H. Freeman and Co., San Francisco, California; Third Edition.

6. M.P. Lisitsa and I.V. Fekeslgazi, Ukrainian Physical Journal, 12, No. 10, p.1701 (1967).

7. G.L. McAllister, M.M. Mann, and L.G. DeShazer, IEE J.Q.E. Vol. QE-6, No. 1, January, 1970.

8. Emil W. Deer, "Toughening a "Glass Jaw", Laser Focus, 38-39, March 1969

9. John F. Kreidl, "The History of the Glass Laser", The Glass Industry, 535-537, October, 1967

APPENDIX I

BIBLIOGRAPHY

The following are additional references obtained since the last report period. O. Kubaschewski provided most of the references and the comments given for some of the references.

The following symbols have been used:

L_A latent heat of fusion of A,

ϵ_A electronegativity of A

ϕ phase diagram study,

* data which have now been superseded,

x data already incorporated in "Metallurgical Thermochemistry", Kubaschewski, O. and Evans, E.LL., Pergamon, London, 1958.

xx data already incorporated in NPL-DCS.7 Report, November, 1970 (two copies enclosed).

( ) solid state

{ } liquid state

1.1.25 Anderson, P.A.M., and Kleppa, O.J., Amer. J. Sci., 1969, 267, 285: ΔH_{974} (formation), sillimanite by solution in $2PbO.B_2O_3$. Data in this paper supersedes some data from the previous one.

1.1.26 Arlyuk, B.I., Zhur. prikl. khim., 1966, 39, 1196: $\langle Na_2O\text{-}SiO_2 \rangle$, $\langle CaO\text{-}Al_2O_3 \rangle$ calculation of ΔH (fusion).

1.1.27 Baird, J.D., and Taylor, J., Trans. Far. Soc., 1958, 54, 526: $CaO\text{-}SiO_2$, ΔG from SiO_2 + C equilibrium, 1450-1550°C, N_{SiO_2} = 0.434-0.660, a_{SiO_2}.

1.1.28 Barany, R., King, E.G., and Todd, S.S., J. Amer. Chem. Soc., 1957, 79, 3639: Ba and Sr silicates, ΔH°_{298} (formation),(solution in HF).

1.1.29 Benz, R., and Schmalzried, H., Z Phys. Chem., N.F., 1961, 29, 77: $\langle PbO\text{-}SiO_2 \rangle$, 640°C, e.m.f., N_{PbO}= 0.50-0.80, ΔG° (formation), $\langle PbSiO_3 \rangle$, $\langle Pb_2SiO_4 \rangle$, $\langle Pb_4SiO_6 \rangle$.

1.1.30 Benz, R. and Wagner, C., J. Phys. Chem., 1961, 65, 1308: $\langle Ca_2SiO_4\text{-}Ca_3Si_2O_7 \rangle$, $\langle Ca_3Si_2O_7\text{-}CaSiO_3 \rangle$, $\langle CaSiO_3\text{-}SiO_2 \rangle$, e.m.f., 700°C, ΔG, $\Delta\bar{G}_{CaO}$.

1.1.31 Billhardt, H.W., Glastech. Ber., 1969, 42, 498: $PbO\text{-}SiO_2$.

1.1.32 Blackburn, P.E., Buchler A., and Stauffer, J.L., J. Phys. Chem., 1966, 70, 2469: Knudsen effusion and weight loss or mass spectrometry ΔG° (formation) 1250°C $\langle Al_4B_2O_9 \rangle$, ΔG° (formation) 1500°C $\langle Al_{18}B_4O_{33} \rangle$.

1.1.33 x Bonnickson, K.R., J. Phys. Chem., 1955, 59, 220:
xx Cp (298-1800K), calcium and magnesium aluminates.

1.1.34 Burylev, B.P., Vasilev, V.V., and Borovick, G.R., Zhur.Fiz.Khim., 1969, 43, 3057: Calculation of ΔG° (formation) for binary liquid mixtures of TiO_2 + CaO, MgO, FeO, Al_2O_3 or SiO_2.

1.1.35 Callow, R.J., Trans. Far. Soc., 1951, 37, 370: $\{PbO\text{-}SiO_2\}$, a_{PbO}, a_{SiO_2}, 1375K derived from volatilization data at 1173-1473K, N_{PbO}= 0.4-1.0, N_{SiO_2} = 0.2-0.9.

1.1.36 Carter, P.T., and Macfarlane, T.G., J. Iron and Steel Inst., 1957, 185, 54: $\{CaO\text{-}Al_2O_3\}$ slags, sulphur equilibration at 1500°C, a_{CaO}, $a_{Al_2O_3}$.

1.1.37 Carter, P.T., and Macfarlane, T.G., J. Iron and Steel Inst., 1957, 185, 62: Gas equilibrium $CO-CO_2-SO_2$ mixture at 1500°C with $CaO-SiO_2$ slags, activities tabulated.

1.1.38 Charette, G.G., and Flengas, S.N., Can. Met. Quart., 1968, 7, 191: $\{PbO-SiO_2\}$, 720-1100°C, e.m.f., a_{PbO}, N_{PbO} = 0.40-0.85, (second law heats and entropies).

1.1.39 Cooper, A.C., Kay, D.A.R., and Taylor, J., Trans. Brit. Ceram. Soc., 1961, 60, 124: $\{Al_2O_3-SiO_2\}$, $\Delta G°$ (formation), 1400-1600°C, equilibrium study using the reaction $3Al_2O_3.2SiO_2 + 6C = 3\ Al_2O_3 + 2SoC = 4CO$.

1.1.40 xx Coughlin, J.P., J. Amer. Chem. Soc., 1956, 78, 5479: $\Delta H°_{298}$ (formation) $\langle CaO.Al_2O_3 \rangle$, $\langle 12CaO.7Al_2O_3 \rangle$, $\langle 3CaO.Al_2O_3 \rangle$ solution calorimetry in HCl.

1.1.41 Coughlin, J.P., and O'Brien, C.J.O., J. Phys. Chem., 1957, 61, 767: Heat contents γ-Ca_2SiO_4 (298-1113K); β-Ca_2SiO_4 (298-1816K).

1.1.42 x Coughlin, J.P., and Orr, R.L., J. Amer. Chem. Soc. , 1953, 75, 530:
xx meta and orthotitanates of barium and strontium; Cp (298-1800K).

1.1.43 Darken, L.S., and Gurry, R.W., "Physical Chemistry of Metals", McGraw-Hill, New York, 1963, 340:
Calculated integral Gibbs energy of mixing for $\{CaO\}$ and $\{SiO_2\}$ at 1600°C.

1.1.44 ∮ De Vries, R.C., Roy, R., and Osborn, E.F., Trans. British Ceram. Soc. 1954, 53, 525: TiO_2-SiO_2.

1.1.45 * Fincham, C.J.B., and Richardson, F.D., Proc. Roy. Soc., 1954, A223, 40: $\{CaO-Al_2O_3\}$, Gas equilibration at 1350-1650°C, using $H_2/CO_2/SO_2$, $\Delta G°$ (formation).

1.1.46 * Flood, H., and Knapp, W.J., J. Amer. Ceram. Soc., 1957, 40, 206: estimate of Gibbs energies of formation for silicates.

1.1.47 Fyffe, W.S., Amer. J. Sci., 1969, 267, 291:
andalusite-sillimanite transition, general discussion of Al_2SiO_5 polymorphism.

1.1.48 Grebenshikov, R.G., and Toropov, N.A., Izv. Akad. Nauk, SSSR, Otdel khim. Nauk, 1962, (4), 545:
$BaO-SiO_2$.

1.1.49 * Haskell and De Vries, R.C., J. Amer. Ceram. Soc., 1964, 47, 202: estimate of Gibbs energy of formation of kyanite.

1.1.50 Ho H., and Yanagase, T., Trans. Japanese Inst. Metals, 1960, 1 (2),115: $\{PbO\text{-}SiO_2\}$, 800-1150°C, N_{SiO_2} = 0.30-0.55, e.m.f., a_{SiO_2}, a_{PbO}.

1.1.51 * Holm, J.L., and Kleppa, O.J., Inorg. Chem. 1966, 5, 698; Amer. Mineral, 1966, 51, 1608; J. Phys. Chem., 1966, 70, 1690: ΔH°_{968} (formation) kyanite, andalusite, sillimanite and mullite by solution in lead and cadmium borates.

1.1.52 Hummel, C., and Schwiete, H.E., Glastechn. Ber., 1959, 32, 413: $\langle Na_2SiO_2 \rangle$, heat of formation, N_{Na_2O} = 0-0.50, (solution in HF at 25°C).

1.1.53 Kelley, K.K., U.S. Bureau Mines Report Investigation, 1961, No. 5901: $CaO\text{-}SiO_2$.

1.1.54 King, E.G., J. Amer. Chem. Soc., 1957, 79, 5437: $\langle Ca_2SiO_4 \rangle$, $\langle Ca_3SiO_7 \rangle$, $\langle CaMgSi_2O_6 \rangle$, $\langle CaAl_2Si_2O_8 \rangle$, Cp(51-298K).

1.1.55 x King, E.G., J. Phys. Chem., 1955, 59, 218:
xx Cp (51-298K), crystalline calcium and magnesium aluminates.

1.1.56 King, E.G., J. Amer. Chem. Soc., 1951, 73, 656; 1952, 74, 4446: $\beta\text{-}Ca_2SiO_4$, Ca_3SiO_5, ΔH°_{298} (formation), also $MnSiO_3$, Fe_2SiO_4 and Zn_2SiO_4, (solution in HF).

1.1.57 Kitayama, K., and Katsura, T., Bull. Chem. Soc. Japan, 1968, 41, 525: ΔG° (formation), 1300°C., Fe_2SiO_4, quenching of melts of FeO + SiO_2 in $CO_2\text{-}H_2$.

1.1.58 Kohler, M.F., Barany, R. and Kelley, K.K., U.S. Bureau Mines Rep. Investigation, 1961, No. 5711: $\langle CaO\text{-}Al_2O_3 \rangle$.

1.1.59 Kozuka, Z., and Samis, C.S., Met. Trans., 1970, 1, 871: $\{PbO\text{-}SiO_2\}$, 900-1000°C, e.m.f., a_{PbO}, a_{SiO_2}, N_{SiO_2} = 0-0.625.

1.1.60 ∮ Kubo, T., and Shinriki, J. Chem. Soc. Japan, Ind. Chem. Section 1951, 54, 268: Ba)-TiO_2.

1.1.61 Larson, H., and Chipman, J., Trans. Met. Soc., AIME, 1953, 197, 1089: Oxygen activity by $CO\text{-}CO_2$ equilibration at 1550°C for one lime-silica slag.

1.1.62 Matsushita, Y., and Goto, K., Tetsu To Hagane Overseas, 1964, 4, (2),128: $\{PbO\text{-}SiO_2\}$, 800-1100°C, oxygen pressure measured in an e.m.f. concentration cell, and activities, Gibbs energy, heat and entropies of mixing are shown graphically.

1.1.63 Orr, R.L., J. Amer. Chem. Soc., 1953, 75, 528: heat content, Fe_2SiO_4, 298-1800K.

1.1.64 Ostvold, T., and Kleppa, O.J., Inorg. Chem., 1969, 8, [1], 78:
{$PbO-SiO_2$}, ΔH_{1173} (formation), N_{SiO_2} = 0.205-0.495, partial heats also determined and combined with activity data to give entropies.

1.1.65 Pankratz, L.B., and Kelley, K.K., U.S. Bur. Mines Rept. Invest., 1964, No. 6370:
high temperature heat contents and entropies of andalusite, kyanite and sillimanite.

1.1.66 Pearce, M.L., J. Amer. Ceram. Soc., 1965, 48, 611:
{Na_2O-SiO_2}, {$Na_2O-B_2O_3$}, calculation of oxygen ion activities in sodium silicate and sodium borate melts.

1.1.67 Pearce, M.L., J. Amer. Ceram. Soc., 1965, 48, 175:
{$Na_2O-B_2O_3$} oxygen ion activity in sodium borate melts, equilibration of melts containing 38.8, 45.4, 49.7, 54.0, wt.% Na_2O with CO_2 at 1 atmosphere.

1.1.68 Pankratz, L.B., Weller, W.W., and Kelley, K.K., U.S. Bur. Mines Rept. Invest., 1963, No. 6287:
low temperature heat capacity and high temperature heat content of mullite.

1.1.69 Richardson, S.W., Bell, P.M., and Gilbert, M.C., Amer. J. Sci., 1968, 266, 513:
kyanite-sillimanite equilibrium, 700-1500°C.

1.1.70 xx Richardson, F.D., Jeffes, J.H.E., and Withers, G., J. Iron and Steel Inst., 1950, 166, 213:
$\Delta G°$ (formation) $CaSiO_3$, $Ca_3Al_2O_6$ (298K); also Al_2SiO_5(29801600), $BaSiO_3$ (29801600), $FeAl_2O_4$ (1100-1400), Na_2SiO_3 (298-1361K).

1.1.71 ϕ Ricker, R.W., and Hummel, F.A., J.Amer. Ceram. Soc., 1951, 34, 271:
TiO_2-SiO_2.

1.1.72 x Roth, W.A., and Troitzsch, H., Z. anorg. allgem. Chem., 1949, 260, 337:
$\Delta H°_{298}$ (formation) Fe_2SiO_4, solution in HF.

1.1.73 ϕ Scholze, H., Z. anorg. allg. Chem., 1956, 284, 272:
$Al_2O_3-B_2O_3$.

1.1.74 Schuhmann, R., and Ensio, P.J., J. Metals, 1951, 401:
($FeO-SiO_2$ slag activities included).

1.1.75 Segnit, E.R., and Gelb, T., Proc. VIIIth Conference Experimental Tech. Mineralogy and Petrology, Novosibirsk, 1968:
$BaO-SiO_2$.

1.1.76 Sharma, R.A., and Richardson, F.D., J. Iron and Steel Inst. 1961, 198, 386:
$\{CaO-Al_2O_3\}$, Gas equilibration at 1500°C using $CO_2/H_2/SO_2$, N_{CaO} = 0.58-0.71, a_{CaO}, $a_{Al_2O_3}$. This paper supersedes the previous one.

1.1.77 Sharma, R.A., and Richardson, F.D., J. Iron and Steel Inst. 1962, 200, 373:
CaS solubility in $\{CaO-SiO_2\}$, 1500°C, N_{CaO} = 0.366-0.577, ΔG, ΔG_{CaO}.

1.1.78 Shibanov, E.V., and Chukhlantsev, V.G., Russian J. Phys. Chem., 1970, 44, (7), 1003:
Calculated ΔH°_{298} (formation): Li_2SiO_3, Li_4SiO_4, K_2SiO_3, $K_2Si_2O_5$, Na_2SiO_3, $Na_2Si_2O_5$, $CaSiO_3$, Ca_2SiO_4, $SrSiO_3$, Sr_2SiO_4, $BaSiO_3$, Ba_2SiO_4

1.1.79 Sridhar, R., and Jeffes, J.H.E., Trans. Inst. Min. Met., 1967, 076, 44:
$\{PbO-SiO_2\}$, e.m.f., 900-1080°C.

1.1.80 ϕ Statton, W.O., J. Chem. Phys., 1951, 19, 33:
$BaO-TiO_2$.

1.1.81 x Stevens, C.G., and Turkdogan, E.I., Trans. Far. Soc., 1955, 51, 356:
Heat of formation of sodium disilicate (solution in HF at 25°C).

1.1.82 xx Taylor, R.W., and Schmalzried, H., J. Phys. Chem., 1964, 68, 2444:
ΔG° (formation), Fe_2SiO_4 also $CaTiO_3$ and $SrTiO_3$.

1.1.83 Tarek El Gammal and H.H. Hohle, Arch. Eisenhüttenw., 1970, 41, 523:
actitivy of sulphur in line-silica slags at 1560°C.

1.1.84 xx Todd, S.S., and Lorenson, R.E., J. Amer. Chem. Soc., 1952, 74, 2043:
metatitanates of barium and strontium, Cp (51-298.16K).

1.1.85 x xx Todd, S.S., and Lorenson, R.E., J. Amer. Chem. Soc., 1952, 74, 3764:
orthotitanates of barium and strontium, Cp (51-309K).

1.1.86 Todd, S.S., J. Amer. Chem. Soc., 1950, 72, 4742:
andalusite, kyanite and sillimanite, Cp (54-298.16K), S°_{298}.

1.1.87 x Todd, S.S., J. Amer. Chem. Soc., 1951, 73, 3277:
β-Ca_2SiO_4, Zn_2SiO_4, Cp (51-298K).

1.1.88 Torgeson, D.R., and Sahama, Th.G., J. Amer. Chem. Soc., 1948, 70, 2156:
$CaSiO_3$, ΔH°_{298} (formation) by HF solution calorimetry.

1.1.89 Tripp, H.P., and King, B.W., J. Amer. Ceram. Soc., 1955, 38, 432:
ΔG° (formation), 0-1700°C., Fe_2SiO_4, $FeSiO_3$, $FeAl_2O_4$, $Ca_2Fe_2O_5$, $CaSiO_3$, $BaSiO_3$, Ca_2SiO_4, CaB_2O_4, CaB_4O_7, Al_2SiO_4, CaB_2O_5, Na_2SiO_3, $Ca_3B_2O_6$, K_2SiO_3.

1.1.90 Waldbaum, D.R., Amer. Mineral., 1965, 50, 186:
Re-evaluation of heats and Gibbs energies of formation for mullite, andalusite, kyanite and sillimanite.

1.1.91 Welch, J.H. and Gutt, W., J. Amer. Ceram. Soc., 1959, 42, 11:
Tricalcium silicate and its stability within the system $CaO-SiO_2$ (high temperature microscopy).

1.1.92 Wygant, J.F., and Kingery, W.D., Bull. Amer. Ceram. Soc., 1952,31, 386:
"Thermodynamics in Ceramics", VI Summary, bibliography and sources of data, Al_2SiO_5, $Ca_3B_2O_6$, $Ca_2B_2O_5$, CaB_2O_4, CaB_4O_7, $CaSiO_3$, $FeSiO_3$, Fe_2SiO_4, $FeTiO_3$, $PbSiO_3$, Pb_2SiO_4.

1.2.20 Elliott, J.F., J. Metals, 1955, 7, (3), 485:
calculation of activities in binary and ternary systems, CaO-FeO-SiO_2.

1.2.21 ∮ Eremin, N.I., Egereva, A.I., Dmitrieva, A.M., and Furfarova, I.B., Zhur. Prikl. Khim, 1970, 43, (1), 18:
CaO-TiO_2-SiO_2 also $CaO.SiO_2$ + Na_2O, Fe_2O_3, MgO or Al_2O_3.

1.2.22 Fulton, C., and Chipman, J., Trans. Met. Soc. AIME, 1954, 200, 1136:
$aSiO_2$ in $\{CaO$-Al_2O_3-$SiO_2\}$, 1425-1700°C, equilibration with CO.

1.2.23 ∮ Gerth, K., and Rehfeld, Silattechnik Deutsche, 1969, 20 (7), 22:
BaO-B_2O_3-SiO_2.

1.2.24 Hlabse, T., and Kleppa, O.J., American Mineral, 1968, 53, 1281:
albite-jadeite, ΔH_{964} (transition), calorimetry in liquid $2PbO.B_2O_3$. $\langle Na_2O$-Al_2O_3-SiO_2 system$\rangle$

1.2.25 ∮ Holland, A.E., and Segnit, E.R., Australian J. Chem., 1966, 19, 905:
Na_2O-ZnO-SiO_2.

1.2.26 Holm, J.L., and Kleppa, O.J., American Miner., 1968, 53, 123:
high temperature albite-low temperature albite, ΔH_{973} (transition), solution calorimetry in lead-cadmium-borate, also heat content of "high albite" at 700°C. $\langle Na_2O$-Al_2O_3-$SiO_2\rangle$.

1.2.27 Kay, D.A.R., and Taylor, J., J. Iron Steel Inst., 1963, 201, 67:
including isoactivity curves for Si in $\{CaO$-Al_2O_3-$SiO_2\}$ at 1500°C.

1.2.28 Kelley, K., Todd, S.S., Orr, R.L., King, E.G., and Bonnickson, U.S. Bur. Mines Report Invest., 1953, No. 4955, "Thermodynamic properties of sodium aluminum and potassium aluminium silicates".

1.2.29 Knapp, W.J., and Flood, H., J. Amer. Ceram. Soc. 1957, 40, 262:
Using the liquidus lines from the phase diagrams, expressions for the activities as functions of composition are developed from structural models of the melts.

$Ca_3(BO_3)_2$ - Ca_2SiO_4	N_{borate} = 0.86-1.00,	1428-1487°C.
$Ca_3(BO_3)_2$ - $CaSiO_3$	N_{borate} = 0.33-1.0,	1185-1482°C.
	$N_{silicate}$ = 0.06-1.0,	1175-1540°C.
$Ca_2B_2O_5$ - Ca_2SiO_4	$N_{B_2O_5}$ = 8.01-1.00,	1240-1312°C.
$Ca(BO_2)_2$ - $CaSiO_3$	N_{borate} = 0.78-1.00,	1050-1162°C.
	$N_{silicate}$ = 0.35-1.00,	1095-1540°C.
$Ca_2B_2O_5$ - $CaSiO_3$	N_{borate} = 0.75-1.00,	1170-1312°C.
	$N_{silicate}$ = 0.34-1.00,	1195-1540°C.

1.2.30 Kalyanram, M.R., Macfarlane, T.G., and Bell, H.B., J. Iron Steel Inst., 1960, 195, 58:
a_{CaO}; 1500°C., sulphur equilibration between $CO-CO_2-SO_2$ and slags at 1500°C. for $CaO-MgO-SiO_2$, $CaO-Al_2O_3-SiO_2$.

1.2.31 ϕ Koppen, N. and Dietzel, A., Naturwissenschaften, 1969, (9), 460:
$BaO-TiO_2-SiO_2$.

1.2.32 Langenberg, F.C., and Chipman, J., Trans. Met. Soc., AIME, 1959, 215, 958:
a_{SiO_2} in $\{CaO-Al_2O_3-SiO_2\}$, 1600°C, 1700°C., equilibration with CO, N_{SiO_2} = 0-0.237.

1.2.33 ϕ Langenberg, F.C., and Chipman, J., J. Amer. Ceram. Soc., 1956, 39, 432:
$CaO-Al_2O_3-SiO_2$.

1.2.34 ϕ Nurse, N.W., and Midgley, J. Iron Steel Inst., 1953, 174, 121:
Na_2O or $K_2O + Al_2O_3 + SiO_2 + CaO$.

1.2.35 ϕ Prince, A.T., J. Amer. Ceram. Soc., 1954, 37, 402:
$CaO-Al_2O_3-SiO_2$.

1.2.36 Richardson, F.D., Jeffes, J.H.E., and Withers, G., J. Iron Steel Inst., 1950, 166, 213:
ΔH°_{298} (formation) $2CaO.Al_2O_3.SiO_2$.

1.2.37 ϕ Roy, R., Roy, D.M., and Osborn, E.F., J. Amer. Ceram. Soc., 1950, 33, 152:
$Li_2O-Al_2O_3-SiO_2$.

1.2.38 ϕ Segnit, E.R., and Holland, A.E., Australian J. Chem., 1970, 23, (6) 1077:
$BaO-ZnO-SiO_2$.

1.2.39 Tarasov, V.V., Turdakin, V.A., Yunitskii, G.A., and Zhdanov, V.M., Zhur. Fiz. Khim., 1967, 41, 430:
Cp, (55-295K), $\langle Na_2O-B_2O_3-SiO_2 \rangle$.

1.2.40 Toop, G.W., and Samis, C.S., Trans. Met. Soc. AIME, 1962, 224, 878:
calculation of activities at 1600°C for Fe^{++}, Ca^{++}, $O^{=}$ in $\{CaO-FeO-SiO_2\}$.

1.2.41 Turkdogan, E.T., Grieveson and Beisler, J.F., Trans. Met. Soc. AIME, 1963, 227, 1258:
a_{SiO_2} in 50% BaO-15% CaO-35% SiO_2 at 1400-1600°C, from quilibrium silicon distribution ratio between slag and graphite saturated iron.

1.2.42 Waldbaum, J., Amer. Ceram. Soc., 1968, 51, 61:
$KAlSi_3O_8$, $NaAlSi_3O_8$, ΔH (fusion), HF solution calorimetry at 497°C., also enthalpies of transition.

1.3.8 Timucin, M., and Morris, A.E., Met. Trsns. 1970, 1, 3193: 1450 and 1550°C, p_{O_2} = 10-11 -1 atmosphere equilibration activities for 0, 5, 10, 20 and 30 wt.% SiO_2 sections.

1.3.9 Timucin, M., Dissertation Abstracts, 1969, 303, (5), 2215: "Phase equilibria and thermodynamic studies of the system $CaO-FeO-Fe_2O_3-SiO_2$.

2. PLATINUM SYSTEMS

2.1 Li-Pt; Na-Pt; K-Pt

2.2 Mg-Pt; Ca-Pt; Sr-Pt; Ba-Pt

2.3 Ce-Pt; Nd-Pt
See Ref. 3.1.37 in the Semi-Annual Report, Jan. 1, 1971.

2.4 B-Pt; Al-Pt; Si-Pt

2.4.5 Ferro, R., Capelli, R., Borsese, A., and Centineo, G., Atti. Accad. Naz., Lincei Rend, C.I., Sci-Fis. Mat. Natur., 1968, 45, 54:
ΔH, (formation), (573-673K), $\langle$ Al-Pt $\rangle$.

2.4.6 See Ref. 3.1.12 in the Semi-Annual Report, Jan. 1, 1971.

2.5 Fe-Pt

2.6 Zn-Pt; Ps-Pt; As-Pt; Sb-Pt

2.6.6 Jena, A.K., and Bever, M.B., Trans. Met. Soc. AIME, 1967, 239, 1861:
Heats of solution at infinite dilution of Ag, Au and Pt in liquid Pb at 623K.

2.6.7 Otopkov, P.P., Gerasimov, Ya.I., and Evseev, A.M., Proc. Acad. Sci., U.S.S.R., Phys. Chem. Section, 1961, p. 839:
{Pt-Pb}, v.p.Pb (973-1148K), N_{Pt} = 0.00-0.89.

2.6.8 Schwerdtfeger, K., Trans. Met. Soc. AIME, 1966, 236, 32:
{Pt-Pb}, e.m.f., 1073-1473K, N_{Pt} = 0.12-0.70, a_{Pb}.

2.6.9 Schwerdtfeger, K., and Zwell, L., Trans. Met. Soc. AIME, 1968, 242, 631:
$\langle$ Rh-Fe $\rangle$, $\langle$ IR-Fe $\rangle$, CO-CO_2 equilibrium at 1200°C.

2.6.10 Kubaschewski, O., "The thermodynamic stability of metallic phases", Battelle Colloquium, Geneva, 1966, McGraw-Hill, 1967, p. 63:
Includes methods of estimation - for example the type of equilibrium diagram formed and therefore the heats of formation of a given alloy, using the size and electronegativity of the components.
For the specific cases of alloys of platinum with the alkali metals or alkaline earth metals, the $(L_A-L_B)/\frac{1}{2}\ (L_A+L_B)$ term is rather negative but is compensated by a rather positive electronegativity term $(\epsilon_A-\epsilon_B)^2$, which makes the application of the method of estimation rather uncertain. However, it appears that at least some of these systems are likely to form large miscibility gaps, even in the liquid state, indicating substantial positive excess Gibbs energies.

3.1.40 Kelley, K.K., U.S. Bureau of Mines, Report Invest. No. 5901, 1962: ΔH°_{298} Mg_2SiO_4, Ca_2SiO_4, Sr_2SiO_4, Ba_2SiO_4, Fe_2SiO_4, Li_2SiO_3, Na_2SiO_3, $MgSiO_3$, $CaSiO_3$, $PbSiO_3$, Li_2Si_2O, K_2SiO_5, $BaSi_2O_5$, $K_2O.4SiO_2$, $3CaO.SiO_2$, $3CaO.2SiO_2$, $2BaO.3SiO_2$, $K_2O.Al_2O_3.3SiO_2$, $CaO.Al_2O_3.2SiO_2$.

3.1.41 Kirkbride, B.J., "The heats of formation of crystalline compounds and of glasses at 25°C"., Pilkington Bros. Ltd., Ormskirk, Lancs, England. Information Report No. I.R. 25, January, 1967: SiO_2 + Li_2O, Na_2O, Rb_2O, Cs_2O, MgO, CaO, Al_2O3 and ternary systems.

3.1.42 Knapp, W.J., and Van Vorst, W.D., J. Amer. Ceram. Soc., 1951, 34, 384: Semempirical methods for estimating the entropies of oxides, silicates and titanates; prediction of reaction equilibria.

3.1.43 Kubaschewski, O., Evans, E.Ll., and Alcock, C.B., "Metallurgical Thermochemistry", 4th Edition, Pergamon, London, 1967; also most recent values of data in the Japanese Edition, 1968.

3.1.44 Kubaschewski, O., "The thermodynamic properties of double oxides", National Physical Laboratory DCS Report 7, November, 1970, (excluding SiO_2 systems).

3.1.45 Kubaschewski, O., "The thermodynamic stability of metallic phases", Battelle Colloquium, Geneva, 1966, McGraw-Hill, 1967, p. 63.

3.1.46 Levin, E.M., Robbins, C.R., and McMurdie, H.F., "Phase diagrams for ceramists", published by The American Ceramic Society, 1964; also E.M. Levin, H.F. McMurdie and F.P. Hall, 1956; E.M. Levin and H.F. McMurdie, 1959.

3.1.47 Matveev, G.M., Rudon, B.L., and Shorshorov, M.Kh., Fiz. Khim. Obrat. Mater. 1969, 6, 94: Calculation of the Gibbs energy of formation at 1000 and 1600K for silicates of Li, Na, Mg, Fe, Mn.

3.1.48 Mott, B.W., "Liquid Immiscibility in Metal Systems", Philosophical Mag. (8th Series) 2, (Feb., 1957).

3.1.49 Richardson, F.D., and Jeffes, J.H.E., J. Iron and Steel Inst., 1948, 160, 261. Cricical evaluation.

3.1.50 Seward, T.P., III, "Phase Diagrams", 1970, Vol. I., Academic Press, N.Y., 298: "Metastable diagrams and their application to glass forming ceramic systems".

APPENDIX II

THERMODYNAMIC INVESTIGATION OF THE INTERACTION OF A LITHIA LASER GLASS WITH PLATINUM

C. A. Alexander, J. S. Ogden, and W. M. Pardue

BATTELLE
Columbus Laboratories

July 22, 1971

INTRODUCTION

In attempting to produce laser glass of the highest purity, one wishes to keep metallic inclusions to a minimum or to eliminate them altogether. The interaction of platinum and molten glass may occur by a number of mechanical and chemical processes. The present study was directed at obtaining sufficient information to attempt to optimize the melting process so that inclusions could be minimized.

The most likely mechanism by which platinum can be dissolved in glass can be envisioned as one whereby oxygen reacts with the platinum to form gaseous platinum oxide, which is then dissolved by the glass. One would expect the platinum concentration in the glass to vary directly with the oxygen partial pressure over the glass melting tank. As one lowers the oxygen pressure, however, the chemical potential of silicon, lithium, calcium, and the minor metallic constituents of the glass rise, and there develops a reaction potential for forming intermetallic compounds with the platinum.

The primary goal of the present investigation was to determine this reaction potential between the metallic constituents of the glass and platinum at low, yet industrially realizable, oxygen partial pressures. A limited effort was directed at determining the platinum content of the laser glass and its thermodynamic activity in the glass.

Experimental

This investigation of the chemical potential of the elemental constituents of laser glass was carried out using a mass spectrometric approach. The mass spectrometer has a great dynamic range and high sensitivity, which allows for the detection of small signals as each component vaporizes at different temperatures.

The observed intensities were much smaller than anticipated; thus, it was impossible to conduct this investigation by an EMF technique or by a transpiration method.

The initial experiment to determine platinum activity and content of the laser glass was conducted in a tungsten Knudsen cell. The interaction of the tungsten cell and the oxides of the glass produced many gaseous tungsten oxides and tungstates.

The method of equilibrating a piece of platinum wire with the laser glass to determine the chemical potential of each constituent in the glass made it possible to carry out the investigation without the interaction of the oxides

The experimental approach was basically one of equilibrating the molten laser glass with platinum for a time long enough to insure that the chemical potential of each of the elements present was the same in the molten glass and in the platinum wire. The oxygen pressure was controlled by using a CO/CO_2 mixture during equilibration.

The equilibration process was carried out in the molybdenum-wound resistance furnace of the transpiration apparatus shown in Figure 1. The laser glass and the platinum wire were placed in a platinum boat inside a platinum liner, insuring that the laser glass had no contact with the alumina tube of the furnace. The CO/CO_2 mixture was introduced just above the platinum boat so that it did not come in contact with the alumina until after it had passed over the sample. The flow of CO and CO_2 was controlled by separate flowmeters so that the CO/CO_2 ratio could be changed to vary the oxygen pressure.

Three separate equilibration runs were made in this apparatus. Pressures of 10^{-6} atm, 10^{-8} atm, and 10^{-10} atm O_2 were chosen for equilibration of the laser glass and the platinum wire. A temperature of 2600 F (1700 K) was maintained for 168 hours at each O_2 pressure. For the 10^{-10} atm O_2 run, the CO/CO_2 ratio was checked by mass spectrometer to ascertain that the inlet-gas mixture was the same as the exit mixture. This check was made to insure that the CO/CO_2 mixture was actually controlling the oxygen pressure, rather than a disproportionation reaction which might be giving off oxygen.

After the equilibration, the sample was cooled and the platinum was separated from the laser glass. The platinum wire was then etched in HF solution for 2 hours to remove any glass particles. The cleaned platinum wire was placed

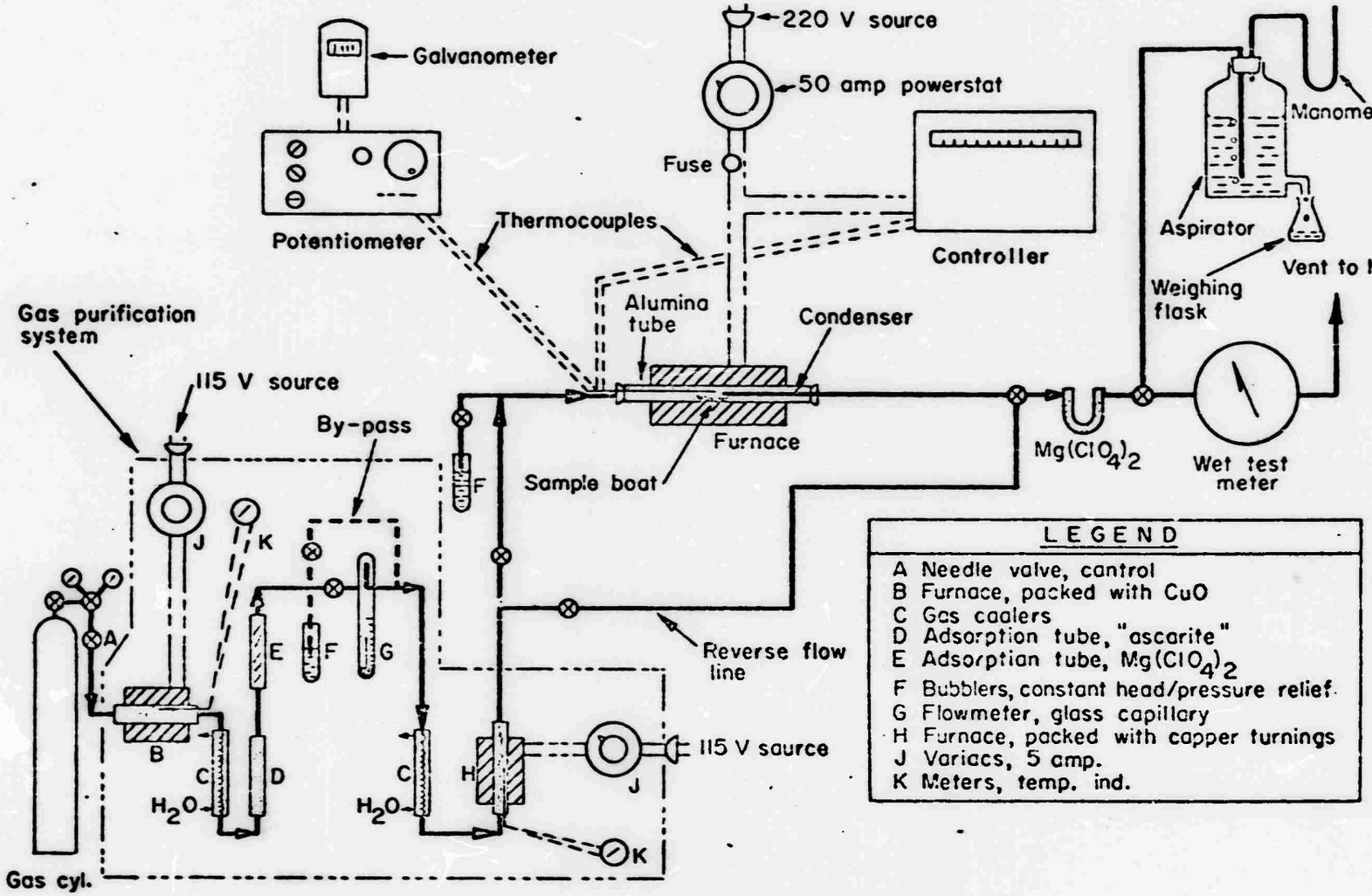

FIGURE 1. THE TRANSPIRATION APPARATUS

in an outgassed BeO liner of a tungsten Knudsen cell, which was then placed in the Nuclide mass spectrometer where the intensities of the constituent ions were measured as a function of temperature. (The constituent atoms diffused into the platinum during equilibration.)

The Nuclide mass spectrometer is a 90° magnetic-sector type with the high-temperature furnace positioned so that the vaporizing beam is perpendicular to the ionizing beam. The mass spectrometer is equipped with a shutter between the Knudsen cell region and the ion source. This shutter, which is normally open, is used to interrupt the vaporizing beam. If the signal ceases or decreases when the shutter is closed, then it is coming from the Knudsen cell and is not part of the background. The observed intensities are transformed into vapor pressure by using the machine calibration constant and a correction for the ionization cross section relative to silver. Cross sections as tabulated by Mann[1] or Drowart[2] were utilized in this study. The calibration constant is determined by completely vaporizing a known quantity of silver from the Knudsen cell. The integrated signal obtained from the measured intensity and time at temperature is the constant. The machine calibration constant for these experiments was 1.0×10^{-15} atm/mv div/°K. The vapor pressure of the platinum also was a check on the machine calibration.

Figure 2 shows the vapor pressure of the platinum calculated by use of the calibration constant of 1.0×10^{-15} atm/mv div/°K and the relative ionization cross sections of the elements calculated by Mann.[1] The solid line is vapor-pressure data taken from Hultgren[3], and the vapor-pressure points from the mass spectrometer data are represented by X's.

Results

From the experiment with the laser glass in the tungsten cell, it is concluded that the laser glass contained 0.6 ppma platinum and that the activity of platinum in the glass is about 10^{-3} at 1700 K. One would expect some reaction between the tungsten Knudsen cell and the platinum, leading to solid-solution formation even at an activity of 10^{-3}. However, if one assumes a diffusion rate of 10^{-7} cm^2/sec for platinum in tungsten, one concludes that the surface of the cell would rapidly come to equilibrium with the platinum gas at its reduced activity

FIGURE 2. VAPOR PRESSURE OF PLATINUM DERIVED FROM MEASUREMENTS COMPARED TO COMPILED VALUE OF HULTGREN

(See following page)

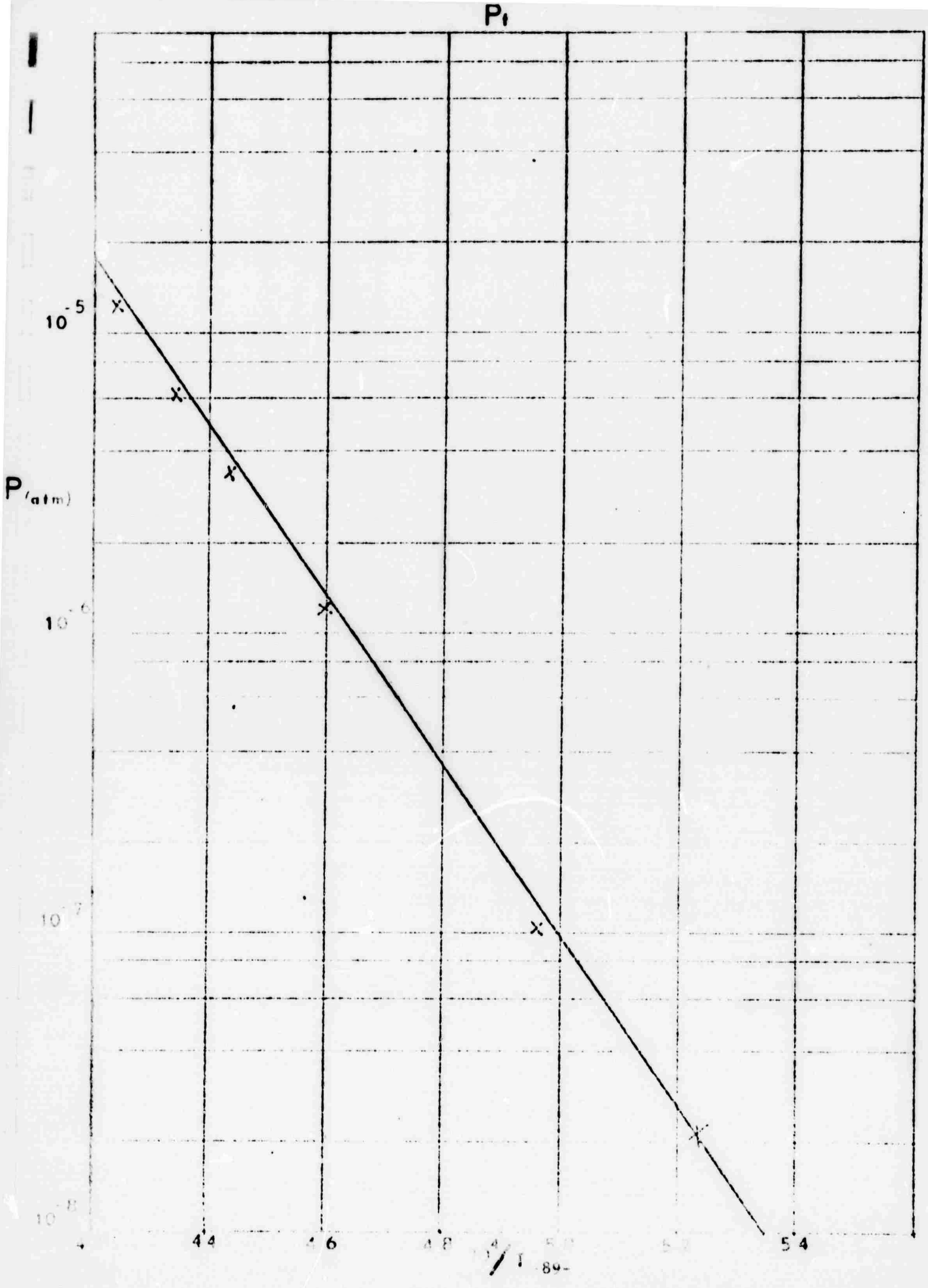
P1
10-5
P(atm)
10-6
10-7
10-8
4.4
4.6
4.8
5.4

and that only a small fraction of the platinum would react with the tungsten. It is considered that the 0.6 ppma is accurate to 0.6 + 0.2, -0.0, based on the integration and the above consideration of platinum diffusion.

The results obtained in the equilibration study are summarized in Table I. The data in Table I are the activities of the metal in the platinum, except for that of aluminum, and the activity of the oxide in the glass at 1700 K. The activity of aluminum in platinum and the activity of the Al_2O_3 in the glass at the equilibration oxygen pressure are reported at 2300 K because aluminum was not detectable below 2100 K in the 10^{-6} atm O_2 and the 10^{-8} atm O_2 runs. The activity of Ca and CaO are not reported for the 10^{-6} atm O_2 experiments because of a calcium contribution from the BeO liner of the Knudsen cell. The 10^{-8} atm O_2 value for calcium is probably a little high for the same reason.

Table 2 lists the amounts of silicon, lithium, aluminum and calcium that diffused into the platinum during equilibration. The quantities were calculated from the intensity of the mass spectrometer signal and the length of time that the signal lasted, similar to the method used for the silver calibration.

Sodium, potassium, iron, cerium, and neodymium were not detected during the experiments, although these elements could be observed in an experiment in which the major constituents were ignored. The problem with the small concentrations is that, while measurements were being made on the major components, the minor components vaporized completely and were not detected. The activities of the lithium, aluminum, and calcium were determined directly from the relation

$$A = \frac{P}{P^\circ} \quad , \qquad (1)$$

where A is activity, P was measured pressure in the mass spectrometer, and P° is the equilibrium pressure for pure component. The activity of the silicon was determined from Equations (2) and (3) because the silicon vaporized from the BeO cell liner.

$$BeO_{(c)} + Si_{(\text{in pt})} = SiO_{(g)} + Be_{(g)} \quad , \qquad (2)$$

where BeO is the crucible material, at unit activity, and the Be and SiO pressures were measured. Then the activity of the Si was calculated from the known values.

TABLE 1. ACTIVITIES OF COMPONENTS IN THE PLATINUM AND GLASS AT 1700 K

	P_{O_2} (atm) for Equilibration		
	10^{-6}	10^{-8}	10^{-10}
P_{O_2} (Knudsen Cell)	10^{-10}	8×10^{-12}	10^{-12}
A_{Si}^{Pt}	6×10^{-14}	5.5×10^{-12}	3×10^{-10}
A_{SiO_2}	0.3	0.28	0.15
A_{Li}^{Pt}	10^{-9}	10^{-8}	2×10^{-8}
A_{Li_2O}	10^{-11}	10^{-9}	6×10^{-10}
A_{Al}^{Pt} at 2300 K	2×10^{-7}	1.4×10^{-6}	1.1×10^{-5}
$A_{Al_2O_3}$ at 2300 K	8×10^{-2}	5×10^{-2}	4×10^{-2}
A_{Ca}^{Pt}		2×10^{-10}	9×10^{-11}
A_{CaO}		1	0.3

TABLE 2. CALCULATED ELEMENTAL PICKUP IN PLATINUM

	P_{O_2} for Equilibration		
PPMW	10^{-6}	10^{-8}	10^{-10}
Si	13	31	48
Li	2	8	14
Al	5	6	22
Ca		9	14

$$Si_{(in\ pt)} + 1/2\ O_{2\ (g)} = SiO_{(g)} \qquad (3)$$

In Equation (3), the SiO and the O_2 are measured quantities and the activity of the Si is calculated. Good agreement was obtained for the activity of Si from Equations (2) and (3). An indication of the manner in which the computation was made can be seen in Figure 3. The oxygen pressure in the Knudsen cell was calculated using Equation (4),

$$WO_2 + 1/2\ O_2 = WO_3\ , \qquad (4)$$

where WO_2 and WO_3 pressures were measured and the O_2 was calculated. At the higher temperatures, the O_2 pressure was also obtained directly from the shuttered O_2 peak and the calibration constant.

The activities of SiO_2, Li_2O, Al_2O_3, and CaO were calculated using the activity of the metal, the equilibrating oxygen pressure, and the equilibrium constant for the formation of the oxide from the JANAF[4] tables. In those cases where the oxide was not listed in the JANAF tables the data for condensed oxides were obtained from Coughlin[5] and for gaseous oxides from Brewer and Rosenblatt[6]. For example, the 10^{-10} atm O_2 equilibration gives a silicon activity of 3×10^{-10}. The equilibrium constant for the reaction

$$Si_{(c)} + O_{2\ (g)} = SiO_{2\ (c)} \qquad (5)$$

at 1/1 and log k = 5.15×10^{18},

$$k = \frac{A_{SiO_2}}{(A_{Si})(A_{O_2})} \quad . \qquad (6)$$

Substituting into Equation (6),

$$5.15 \times 10^{18} = \frac{A_{SiO_2}}{(3 \times 10^{-10})(10^{-10})}$$

$$A_{SiO_2} = (5.15 \times 10^{18})(3 \times 10^{-10})(10^{-10}) = 15 \times 10^{-2}$$

$$A_{SiO_2} = 0.15$$

FIGURE 3. ACTIVITY OF SILICON COMPUTED FROM THE RELATION,

$Si\ (in\ pt) + 1/2\ O_2\ (g) = SiO\ (g)$, for the $10^{-8}\ O_2$ Equilibration

(See following page)

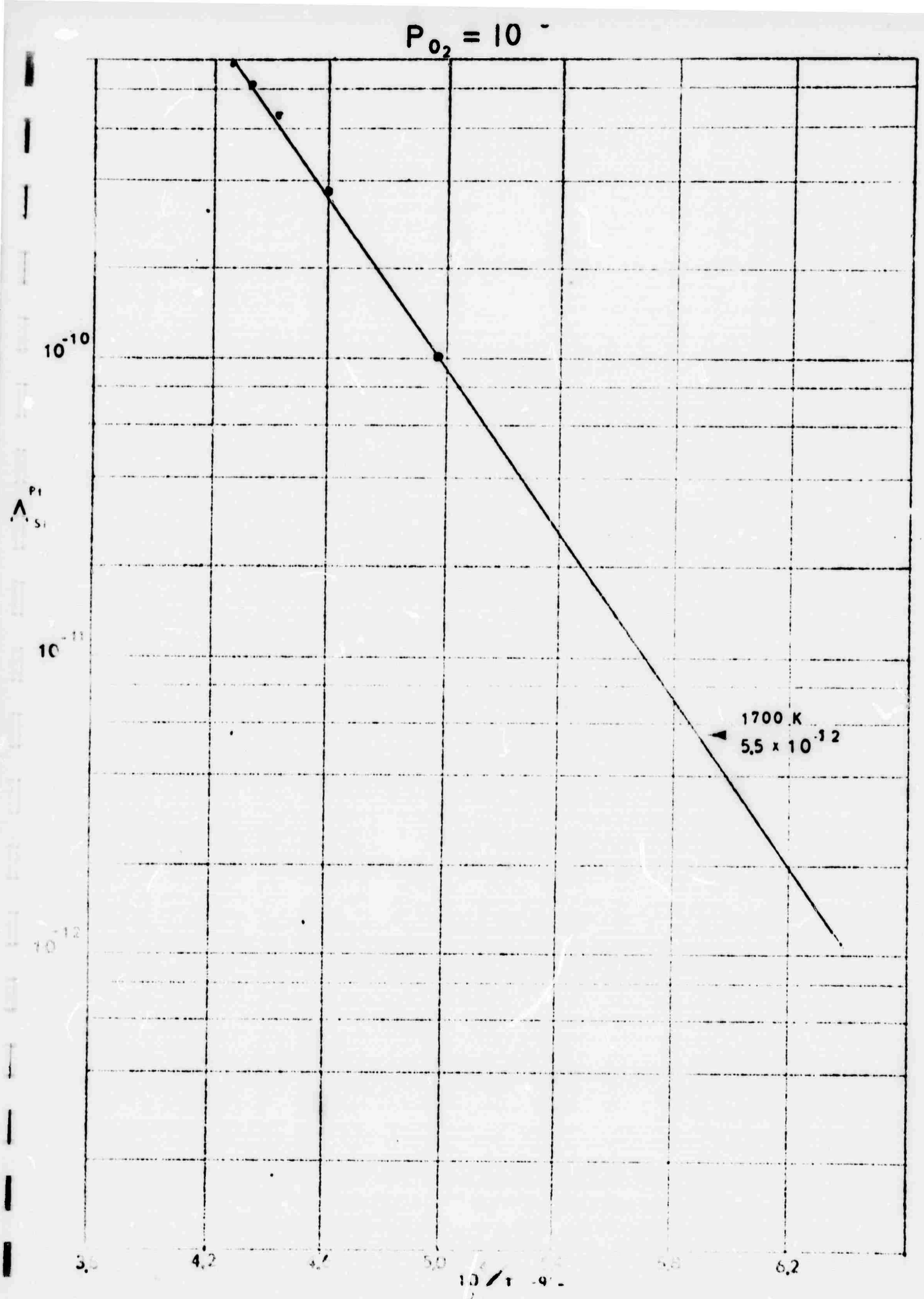
$P_{O_2} = 10^{-}$
10^{-10}
A^{Pt}_{Si}
10^{-11}
1700 K
$5,5 \times 10^{-12}$
10^{-12}
4,2
6,2

The free energy values used to derive the values in Table 1 are given in Table 3.

Conclusions

The data obtained and outlined in Tables 1 and 2 indicate that platinum and laser glass are still compatible at an oxygen pressure as low as 10^{-10} atmosphere. It had been hoped that Henry's law would apply to the very dilute solution of elements in platinum. That such is not the case may be seen from the data in Table 4 where, based on the previous data, the Henry's law constant $a = kX_o$ has been calculated. In this expression, a is the activity taken from Table 1 and X_o is the atom fraction, derived from the concentration given in Table 2. Had Henry's law been obeyed, the data would have been much more amenable to extrapolation and one might be able to predict at what oxygen potential the concentration of silicon in platinum would reach a level such as to cause structural damage to the platinum. If, in noting the trend in the Henry's law constants with concentration, one considers that a value of the constant for silicon of between 10^{-5} and 10^{-4}, say 3×10^{-5}, might be a reasonable estimate for the magnitude of the constant when the concentration is 0.1 atom percent silicon in platinum. This would indicate that if the silicon activity reached 3×10^{-8}, one could expect 1000 ppma of silicon in the platinum. Based on the silicon activities given in Table 1, one might expect the silicon activity to be 3×10^{-8} at an oxygen pressure of 10^{-12} atmosphere; hence, it would appear that one might go to a pressure as low as this and still maintain the structural integrity of the platinum crucible. Examination of the platinum used in the equilibration studies showed no evidence of grain-boundary attack either visually or by electron probe, nor does the scanning electron microscope reveal any evidence which would indicate that a reaction of any extent occurred.

The evidence indicates that Henry's law does not apply to the platinum, and probably does not apply to the glass; hence, there is a need for more information before one can accurately predict the amount of platinum one would expect in the glass due to nonmechanical effects. There is evidence that atmosphere control should lead to a glass with a concentration of less than one part per billion, however. This conclusion awaits experimental verification for, although one can estimate the magnitude of the reaction involving solubility of the gaseous platinum oxide, there is no certainty that this is the only reaction, nor that intrinsic solubility will supply a finite amount of platinum to the glass.

TABLE 3. FREE ENERGIES OF FORMATION USED IN THIS INVESTIGATION AND THE REFERENCE STATE

Component	-ΔG at 1700 K, kcal/mole
SiO_2 (q)	145.6
SiO (g)	58.2
Li_2O (l)	85.3
Al_2O_3 (c)	270.6
CaO (c)	108.2
BeO (c)	103.5
	-ΔG at 2000 K
NdO (g)	62.3
Nd_2O_3 (c)	264.0
CeO (g)	48.1
CeO_2 (c)	142.1

TABLE 4. HENRY'S LAW CONSTANTS FOR CONSTITUENTS IN PLATINUM

Element	P_{O_2} for Equilibration 10^{-6}	10^{-8}	10^{-10}
Si	7×10^{-10}	2×10^{-8}	9×10^{-7}
Li	2×10^{-5}	4×10^{-5}	5×10^{-5}
Al	6×10^{-3}	3×10^{-2}	7×10^{-2}
Ca	--	5×10^{-6}	1×10^{-6}

REFERENCES

1. Mann, "Ionization Cross Sections of the Elements Calculated from Mean-Square Radii of Atomic Orbitals", J. Chem. Phys. 46, 1646-51, 1967.

2. Drowart and Goldfinger, "Investigation of Inorganic Systems at High Temperature by Mass Spectrometer", Angewandte Chemie, 6, 581-648, 1967.

3. Hultgren, Orr, and Kelley, "Selected Values of Thermodynamic Properties".

4. JANAF Interim Thermochemical Tables.

5. Bu. Mines Bulletin 542 (1954).

6. Leo Brewer and Gerd Rosenblatt, "Dissociation Energies of Gaseous Monoxides", Advances in High Temperature Chemistry, V-2.

APPENDIX A

Due to the very low values of activities of the constituent elements in [illegible] the uncertainties in the data are somewhat higher than might ordinarily be [illegible] from a mass spectral investigation. With the effusion cell geometry employed gaseous species could be determined if their partial pressures were 10^{-11} atm or higher. Neither NdO nor CeO were observed at 2000 K, and from these values one can assign an upper limit to the activities of neodymium and cerium but at 2000 K not at 1700 K. Based on observation of Al_2O_3 in the glass where the temperature coefficient of activity was found to be quite small one might expect that the upper limit values given at 2000 K maybe a reasonable value to use at 1700 K also. In determining best values more weight was given to the 10^{-10} equilibration run for these reasons. First, there was more of the constituents in the platinum hence signals were more intense and measurements could be performed over a larger temperature range. The second reason is that experience gained in making those kind of determinations from the first two runs enabled a more systematic approach to be taken in that one could anticipate at what temperature to look for the various species and little time was expended in going from mass to mass and from one temperature to another. The third factor is that all possible signal contributions from the beryllia liner were believed to be eliminated by the very high temperatures outgassing prior to run three. There is little doubt the calcia observed in the early runs came from the crucible and it is possible there was a small contribution of silica also. The activity values given reflect the precision in the mass spectral data but do not allow for any uncertainty inherent in the reference data from the JANAF tables. It is [illegible] that for most cases uncertainties in reference data could introduce an uncertainty of at least 50 percent in the number reported.

TABLE A-1. RECOMMENDED VALUES FOR ACTIVITIES IN LITHIA LASER GLASS AT 1700 K

Component	Activity	Mole Fraction in Glass
SiO_2	2×10^{-1}	0.59
Li_2O	6×10^{-10}	0.28
CaO	1×10^{-1}	0.10
Al_2O_3	2×10^{-2}	0.025
CeO_2	$< 10^{-4}$	0.0016
Nd_2O_3	$< 10^{-3}$	0.005

APPENDIX III: CALCULATION OF P_{O_2} REQUIRED FOR Pt FAILURE

The thermodynamic calculatiens below estimate the P_{O_2} required for Pt metal failure in centact with the Li_2O-CaO-SiO_2-Nd_2O_3 laser glass. Pt "failure" can be expressed from a chemical point of view by Reaction (1). Silicon is used as an example.

$$Si\ (X_{Si}^{Pt}\ \text{in failed Pt}) + O_2\ (\text{gas},\ P_{O_2}) \rightarrow SiO_2\ (X_{SiO_2}^{glass}\ \text{in glass sol'n});$$

$$T = 1700°K \qquad R_x\ (1)$$

When these three phases are in equilibrium at the appropriate mole fractions and partial pressure, the Pt will have "failed" by definition.

Equilibrium occurs when the Gibb's free energy for Reaction (1) ($\Delta F_{(1)}$) is zero.

$$\Delta F = \Delta F^\circ + RT \ln \left| \frac{A_{SiO_2}^{glass}}{(A_{S_1}^{Pt})\ (P_{O_2})} \right| = 0 \qquad \text{Eq. II-1}$$

The P_{O_2} required for $\Delta F \leq 0$ is desired. $\Delta F^\circ_{(1)} = \Delta F^\circ_f\ (SiO_{2(2)}) = -137{,}931$ cal/mole at 1700°K (2600°F).

For glass composition #5, $X_{SiO_2}^{glass} = 0.593$ and the $A_{SiO_2}^{glass}$ has been experimentally determined; because "failure" was not observed above $P_{O_2} = 10^{-10}$ atm., let $A_{SiO_2}^{glass} = 0.15$ for the calculatien. The mole fractions of the glass constituents are not being changed in erder te avoid Pt failure so these mole fractiens and correspending activities will remain constant for the calculations.

The $A_{MeO_x}^{glass}$'s are available at 1700°K for SiO_2, Li_2O and CaO. Insufficient data is available to estimate $A_{Al_2O_3}^{glass}$.

There are two ways of estimating the A_{Si}^{Pt} at failure, the last parameter necessary in order to calculate P_{O_2} required for failure. The A_{Si}^{Pt} can be estimated knowing the $\Delta F^{o}f$ $(SiPT_x)$, A_{Si}^{Pd}, A_{Si}^{Re}, or A_{Si}^{Ni} as done in Appendix IV of the Semi-Annual Report[3]. Based upon this empirical data, the A_{Si}^{Pt} at failure has been estimated to be 10^{-5} at 1533°K. These data could be temperature corrected from 1533°K to 1700°K by assuming that $T \log A_{Me}^{Rt}$ is not a function of temperature. This can be demonstrated by considering the reaction:

$$Me\ (pure) \rightarrow Me\ (in\ Pt\ soln.) \qquad Rx\ (2)$$

For Rx (2), $\Delta F_{②} = \Delta H_{②} - T\Delta S_{②}$. $\Delta S_{②} \approx 0$ because the degree of disorder is is similar between solids and between solids and liquids; therefore, $\Delta F_{②}$ is not a strong F (T). Also note:

$$\Delta F_{②} = + RT \ln A_{Al_2O_3}^{glass}$$

Therefore, $T \log A_{Al_2O_3}^{glass}$ is not a strong f (t). Using this relation, the A_{Me}^{Pt} at 1700°K can be calculated knowing A_{Al}^{Pt} at 1533°K. Consider A_{Si}^{Pt} as an example:

$$(1533^{o}K) \log A_{Si}^{Pt} @ 1533^{o}K = (1700^{o}K) \log A_{Si}^{Pt} @ 1700^{o}K$$

$$\log A_{Si}^{Pt} @ 1700^{o}K = \frac{1533}{1700} (10^{-5}) = 0.9 \times 10^{-5} \sim 10^{-5}$$

Since the estimated value of the A_{Me}^{Pt} @ 1533°K is not accurate to more than one order of magnitude, the A_{Me}^{Pt} @ 1533°K A_{Me}^{Pt} @1700°K.

Using the above values and Eq.III-1, the P_{O_2} required for failure is calculated: $-145{,}600 + (1.987)(2.303)(1700^{o}K) \log_{10} \left[\frac{0.15}{(10^{-5})(P_{O_2})} \right] = 0$

Therefore, $P_{O_2} \sim 10^{-13.0}$ atm. is order for failure to occur.

The same calculation is done for the other oxides and metals. The data used is presented in Table III-1 and the P_{O_2}'s are summarized in Table 7 of this report.

The other method of estimating the A_{Me}^{Pt} at failure assumes that ~/at.% of the metal (Me) can be dissolved in the Pt before failure would be expected. The A_{Me}^{Pt} is related to the mold fraction (X_{Me}^{Pt}) by the relation $A_{Mc}^{Pt} = \varepsilon_{Me}^{Pt} X_{Me}^{Pt}$ where ε_{Me}^{Pt} is the activity coefficient as empirically determined and listed in Table 4. Table III-2 lists the data used in Quation III-1 to calculate P_{O_2} required for failure and the obtained P_{O_2} values.

TABLE III-1

CALCULATION OF P_{O_2} REQUIRED FOR Pt FAILURE ASSUMING A_{Me}^{Pt}'s FROM REF. 3. T = 1700°K = 2600°F

Element (Me)	$A_{MeO_x}^{glass}$	A_{Me}^{Pt}	ΔF_f°(MeO) (cal/mole)	P_{O_2} Required for Pt Failure
Si	0.15	10^{-5}	-145,600	$\leq 10^{-13.0}$ atm.
Li	6×10^{-10}	10^{-6}	- 85,431	$\leq 10^{-13.8}$ atm.
Al	1.29×10^{-2}	10^{-8}	-269,389	$\leq 10^{-12.6}$ atm.
Ca	0.1	10^{-4}	-108,160	$\leq 10^{-20.9}$ atm.

TABLE III-2

CALCULATION OF P_{O_2} REQUIRED FOR Pt FAILURE ASSUMING

$X_{Me}^{Pt} = 0.01$ and γ_{Me}^{Pt} ($X_{Me}^{Pt} = 0.01 = \gamma_{Me}^{Pt}$ from Table 4 of Report.

$T = 1700^{\circ}K = 2600^{\circ}F.$

Element (Me)	A_{MeO_x}	X_{Me}^{Pt}	γ_{Me}^{Pt}	$\Delta F^{\circ}_f(MeO_x)$ cal/mole	P_{O_2} required for Pt Failure
Si	0.15	0.01	9×10^{-7}	-145,600	$\geq 10^{-11.5}$ atm.
Li	6×10^{-10}	0.01	5×10^{-5}	- 85,431	$\geq 10^{-14.8}$ atm.
Ca	0.1	0.01	1×10^{-6}	-108,160	$\geq 10^{-21.2}$ atm.

* This value has been temperature corrected for 1700°K.